Search for R-Parity Violating Decays of Scalar Fermions at LEP

The OPAL Collaboration

Abstract

A search for pair-produced scalar fermions under the assumption that R-parity is not conserved has been performed using data collected with the OPAL detector at LEP. The data samples analysed correspond to an integrated luminosity of about 610 pb^{-1} collected at centre-of-mass energies of $\sqrt{s} = 189-209$ GeV. An important consequence of R-parity violation is that the lightest supersymmetric particle is expected to be unstable. Searches for R-parity violating decays of charged sleptons, sneutrinos and squarks have been performed under the assumptions that the lightest supersymmetric particle decays promptly and that only one of the R-parity violating couplings is dominant for each of the decay modes considered. Such processes would yield final states consisting of leptons, jets, or both, with or without missing energy. No significant signal-like excess of events has been observed with respect to the Standard Model expectations. Limits on the production cross-sections of scalar fermions in R-parity violating scenarios are obtained. Constraints on the supersymmetric particle masses are also presented in an R-parity violating framework analogous to the Constrained Minimal Supersymmetric Standard Model.

The OPAL Collaboration

G. Abbiendi[2], C. Ainsley[5], P.F. Åkesson[3], G. Alexander[22], J. Allison[16], P. Amaral[9],
G. Anagnostou[1], K.J. Anderson[9], S. Arcelli[2], S. Asai[23], D. Axen[27], G. Azuelos[18,a], I. Bailey[26],
E. Barberio[8,p], R.J. Barlow[16], R.J. Batley[5], P. Bechtle[25], T. Behnke[25], K.W. Bell[20], P.J. Bell[1],
G. Bella[22], A. Bellerive[6], G. Benelli[4], S. Bethke[32], O. Biebel[31], O. Boeriu[10], P. Bock[11],
M. Boutemeur[31], S. Braibant[8], L. Brigliadori[2], R.M. Brown[20], K. Buesser[25], H.J. Burckhart[8],
S. Campana[4], R.K. Carnegie[6], B. Caron[28], A.A. Carter[13], J.R. Carter[5], C.Y. Chang[17],
D.G. Charlton[1], A. Csilling[29], M. Cuffiani[2], S. Dado[21], A. De Roeck[8], E.A. De Wolf[8,s],
K. Desch[25], B. Dienes[30], M. Donkers[6], J. Dubbert[31], E. Duchovni[24], G. Duckeck[31],
I.P. Duerdoth[16], E. Etzion[22], F. Fabbri[2], L. Feld[10], P. Ferrari[8], F. Fiedler[31], I. Fleck[10], M. Ford[5],
A. Frey[8], A. Fürtjes[8], P. Gagnon[12], J.W. Gary[4], G. Gaycken[25], C. Geich-Gimbel[3],
G. Giacomelli[2], P. Giacomelli[2], M. Giunta[4], J. Goldberg[21], E. Gross[24], J. Grunhaus[22],
M. Gruwé[8], P.O. Günther[3], A. Gupta[9], C. Hajdu[29], M. Hamann[25], G.G. Hanson[4], K. Harder[25],
A. Harel[21], M. Harin-Dirac[4], M. Hauschild[8], C.M. Hawkes[1], R. Hawkings[8], R.J. Hemingway[6],
C. Hensel[25], G. Herten[10], R.D. Heuer[25], J.C. Hill[5], K. Hoffman[9], D. Horváth[29,c],
P. Igo-Kemenes[11], K. Ishii[23], H. Jeremie[18], P. Jovanovic[1], T.R. Junk[6], N. Kanaya[26],
J. Kanzaki[23,u], G. Karapetian[18], D. Karlen[26], K. Kawagoe[23], T. Kawamoto[23], R.K. Keeler[26],
R.G. Kellogg[17], B.W. Kennedy[20], D.H. Kim[19], K. Klein[11,t], A. Klier[24], S. Kluth[32],
T. Kobayashi[23], M. Kobel[3], S. Komamiya[23], L. Kormos[26], T. Krämer[25], P. Krieger[6,l], J. von
Krogh[11], K. Kruger[8], T. Kuhl[25], M. Kupper[24], G.D. Lafferty[16], H. Landsman[21], D. Lanske[14],
J.G. Layter[4], A. Leins[31], D. Lellouch[24], J. Letts[o], L. Levinson[24], J. Lillich[10], S.L. Lloyd[13],
F.K. Loebinger[16], J. Lu[27,w], J. Ludwig[10], A. Macpherson[28,i], W. Mader[3], S. Marcellini[2],
A.J. Martin[13], G. Masetti[2], T. Mashimo[23], P. Mättig[m], W.J. McDonald[28], J. McKenna[27],
T.J. McMahon[1], R.A. McPherson[26], F. Meijers[8], W. Menges[25], F.S. Merritt[9], H. Mes[6,a],
A. Michelini[2], S. Mihara[23], G. Mikenberg[24], D.J. Miller[15], S. Moed[21], W. Mohr[10], T. Mori[23],
A. Mutter[10], K. Nagai[13], I. Nakamura[23,V], H. Nanjo[23], H.A. Neal[33], R. Nisius[32], S.W. O'Neale[1],
A. Oh[8], A. Okpara[11], M.J. Oreglia[9], S. Orito[23,*], C. Pahl[32], G. Pásztor[4,g], J.R. Pater[16],
G.N. Patrick[20], J.E. Pilcher[9], J. Pinfold[28], D.E. Plane[8], B. Poli[2], J. Polok[8], O. Pooth[14],
M. Przybycień[8,n], A. Quadt[3], K. Rabbertz[8,r], C. Rembser[8], P. Renkel[24], J.M. Roney[26],
S. Rosati[3], Y. Rozen[21], K. Runge[10], K. Sachs[6], T. Saeki[23], E.K.G. Sarkisyan[8,j], A.D. Schaile[31],
O. Schaile[31], P. Scharff-Hansen[8], J. Schieck[32], T. Schörner-Sadenius[8], M. Schröder[8],
M. Schumacher[3], C. Schwick[8], W.G. Scott[20], R. Seuster[14,f], T.G. Shears[8,h], B.C. Shen[4],
P. Sherwood[15], G. Siroli[2], A. Skuja[17], A.M. Smith[8], R. Sobie[26], S. Söldner-Rembold[16,d],
F. Spano[9], A. Stahl[3], K. Stephens[16], D. Strom[19], R. Ströhmer[31], S. Tarem[21], M. Tasevsky[8],
R.J. Taylor[15], R. Teuscher[9], M.A. Thomson[5], E. Torrence[19], D. Toya[23], P. Tran[4], I. Trigger[8],
Z. Trócsányi[30,e], E. Tsur[22], M.F. Turner-Watson[1], I. Ueda[23], B. Ujvári[30,e], C.F. Vollmer[31],
P. Vannerem[10], R. Vértesi[30], M. Verzocchi[17], H. Voss[8,q], J. Vossebeld[8,h], D. Waller[6], C.P. Ward[5],
D.R. Ward[5], P.M. Watkins[1], A.T. Watson[1], N.K. Watson[1], P.S. Wells[8], T. Wengler[8],
N. Wermes[3], D. Wetterling[11] G.W. Wilson[16,k], J.A. Wilson[1], G. Wolf[24], T.R. Wyatt[16],
S. Yamashita[23], D. Zer-Zion[4], L. Zivkovic[24]

[1]School of Physics and Astronomy, University of Birmingham, Birmingham B15 2TT, UK
[2]Dipartimento di Fisica dell' Università di Bologna and INFN, I-40126 Bologna, Italy

[3]Physikalisches Institut, Universität Bonn, D-53115 Bonn, Germany

[4]Department of Physics, University of California, Riverside CA 92521, USA

[5]Cavendish Laboratory, Cambridge CB3 0HE, UK

[6]Ottawa-Carleton Institute for Physics, Department of Physics, Carleton University, Ottawa, Ontario K1S 5B6, Canada

[8]CERN, European Organisation for Nuclear Research, CH-1211 Geneva 23, Switzerland

[9]Enrico Fermi Institute and Department of Physics, University of Chicago, Chicago IL 60637, USA

[10]Fakultät für Physik, Albert-Ludwigs-Universität Freiburg, D-79104 Freiburg, Germany

[11]Physikalisches Institut, Universität Heidelberg, D-69120 Heidelberg, Germany

[12]Indiana University, Department of Physics, Bloomington IN 47405, USA

[13]Queen Mary and Westfield College, University of London, London E1 4NS, UK

[14]Technische Hochschule Aachen, III Physikalisches Institut, Sommerfeldstrasse 26-28, D-52056 Aachen, Germany

[15]University College London, London WC1E 6BT, UK

[16]Department of Physics, Schuster Laboratory, The University, Manchester M13 9PL, UK

[17]Department of Physics, University of Maryland, College Park, MD 20742, USA

[18]Laboratoire de Physique Nucléaire, Université de Montréal, Montréal, Québec H3C 3J7, Canada

[19]University of Oregon, Department of Physics, Eugene OR 97403, USA

[20]CLRC Rutherford Appleton Laboratory, Chilton, Didcot, Oxfordshire OX11 0QX, UK

[21]Department of Physics, Technion-Israel Institute of Technology, Haifa 32000, Israel

[22]Department of Physics and Astronomy, Tel Aviv University, Tel Aviv 69978, Israel

[23]International Centre for Elementary Particle Physics and Department of Physics, University of Tokyo, Tokyo 113-0033, and Kobe University, Kobe 657-8501, Japan

[24]Particle Physics Department, Weizmann Institute of Science, Rehovot 76100, Israel

[25]Universität Hamburg/DESY, Institut für Experimentalphysik, Notkestrasse 85, D-22607 Hamburg, Germany

[26]University of Victoria, Department of Physics, P O Box 3055, Victoria BC V8W 3P6, Canada

[27]University of British Columbia, Department of Physics, Vancouver BC V6T 1Z1, Canada

[28]University of Alberta, Department of Physics, Edmonton AB T6G 2J1, Canada

[29]Research Institute for Particle and Nuclear Physics, H-1525 Budapest, P O Box 49, Hungary

[30]Institute of Nuclear Research, H-4001 Debrecen, P O Box 51, Hungary

[31]Ludwig-Maximilians-Universität München, Sektion Physik, Am Coulombwall 1, D-85748 Garching, Germany

[32]Max-Planck-Institute für Physik, Föhringer Ring 6, D-80805 München, Germany

[33]Yale University, Department of Physics, New Haven, CT 06520, USA

[a] and at TRIUMF, Vancouver, Canada V6T 2A3

[c] and Institute of Nuclear Research, Debrecen, Hungary

[d] and Heisenberg Fellow

[e] and Department of Experimental Physics, Lajos Kossuth University, Debrecen, Hungary

[f] and MPI München

[g] and Research Institute for Particle and Nuclear Physics, Budapest, Hungary

[h] now at University of Liverpool, Dept of Physics, Liverpool L69 3BX, U.K.

[i] and CERN, EP Div, 1211 Geneva 23

[j] and Manchester University

^{k} now at University of Kansas, Dept of Physics and Astronomy, Lawrence, KS 66045, U.S.A.

^{l} now at University of Toronto, Dept of Physics, Toronto, Canada

^{m} current address Bergische Universität, Wuppertal, Germany

^{n} now at University of Mining and Metallurgy, Cracow, Poland

^{o} now at University of California, San Diego, U.S.A.

^{p} now at Physics Dept Southern Methodist University, Dallas, TX 75275, U.S.A.

^{q} now at IPHE Université de Lausanne, CH-1015 Lausanne, Switzerland

^{r} now at IEKP Universität Karlsruhe, Germany

^{s} now at Universitaire Instelling Antwerpen, Physics Department, B-2610 Antwerpen, Belgium

^{t} now at RWTH Aachen, Germany

^{u} and High Energy Accelerator Research Organisation (KEK), Tsukuba, Ibaraki, Japan

^{v} now at University of Pennsylvania, Philadelphia, Pennsylvania, USA

^{w} now at TRIUMF, Vancouver, Canada

* Deceased

1 Introduction

In Supersymmetric (SUSY) [1] models, each elementary particle is accompanied by a supersymmetric partner whose spin differs by half a unit. Many of the searches for these supersymmetric particles ("sparticles") are performed within the Minimal Supersymmetric extension of the Standard Model (MSSM) [2], assuming R-parity conservation. R-parity [3] is a multiplicative quantum number defined as $R_p = (-1)^{2S+3B+L}$ where S, B and L are the spin, baryon and lepton numbers of the particle, respectively. R-parity discriminates between ordinary and supersymmetric particles: $R_p = +1$ for Standard Model particles and $R_p = -1$ for their supersymmetric partners. R-parity conservation implies that supersymmetric particles are always pair-produced and always decay through cascade decays to ordinary particles and the lightest supersymmetric particle (LSP). In this context, the LSP is often assumed to be the lightest neutralino, $\tilde{\chi}_1^0$, which is then expected to be stable and to escape detection due to its weakly interacting nature. The characteristic signature of the supersymmetric R-parity conserving decays is therefore missing energy.

If R-parity is violated, sparticles can be pair-produced but may decay directly to Standard Model particles. Scalar neutrinos could also be singly-produced via an s- or t-channel sneutrino exchange [4, 5]. In the present paper, the possible direct manifestations of R-parity breaking couplings via pair-production of sparticles and their subsequent R-parity violating decays to Standard Model particles are studied. The signatures sought in the analyses of this paper therefore differ from the missing energy signatures of R-parity conserving processes.

R-parity violating interactions of the particles of the MSSM are parametrised with a gauge-invariant superpotential that includes the following Yukawa coupling terms [6]:

$$W_{RPV} = \lambda_{ijk} L_i L_j \overline{E}_k + \lambda'_{ijk} L_i Q_j \overline{D}_k + \lambda''_{ijk} \overline{U}_i \overline{D}_j \overline{D}_k + \epsilon_i L_i H_2, \qquad (1)$$

where i, j, k are the generation indices of the superfields L, Q, E, D and U. L and Q are lepton and quark left-handed doublets, respectively. $\overline{E}$, $\overline{D}$ and $\overline{U}$ are right-handed singlet charge-conjugate superfields for the charged leptons, down- and up-type quarks, respectively. H_2 is the Higgs doublet superfield with a weak hypercharge $Y = 1$. The last term in (1) which mixes the lepton and Higgs superfields is not considered in this paper. The interactions corresponding to these superpotential terms are assumed to respect the gauge symmetry $SU(3)_C \times SU(2)_L \times U(1)_Y$ of the Standard Model. The λ_{ijk} are non-vanishing only if $i < j$, so that at least two different generations are coupled in the purely leptonic vertices. The λ''_{ijk} are non-vanishing only for $j < k$. The λ and λ' couplings both violate lepton number conservation and the λ'' couplings violate baryon number conservation. There are nine λ couplings for the triple lepton vertices, 27 λ' couplings for the lepton-quark-quark vertices and nine λ'' couplings for the triple quark vertices. There are therefore a total of 45 R-parity violating couplings.

In the Constrained Minimal Supersymmetric Standard Model (CMSSM), which assumes a common gaugino mass, $m_{1/2}$, and a common sfermion mass, m_0, at the Grand Unification (GUT) scale, all sparticle masses and R-parity conserving couplings are completely determined by m_0 and a set of three parameters: M_2, the SU(2) gaugino mass parameter at electroweak scales[1], μ, the mixing parameter of the two Higgs doublets and $\tan\beta = v_2/v_1$, the ratio of the vacuum expectation values for the two Higgs doublets.

---

[1] M_1, the U(1) gaugino mass at electroweak scales, is related to M_2 by the usual gauge unification condition: $M_1 = \frac{5}{3}\tan^2\theta_W M_2$.

From low energy experiments, there exist several upper bounds on the R-parity violating Yukawa couplings, λ, $\lambda^{'}$ and $\lambda^{''}$. A list of upper limits on individual couplings can be found in [5, 7–15]. The experimental limits on processes such as proton decay imply that it is reasonable to assume that no more than one of the 45 couplings is significantly different from zero [6].

This paper describes searches for R-parity violating decays of pair-produced scalar fermions ("sfermions"), such as the charged and neutral scalar leptons ($\tilde{\ell}$ and $\tilde{\nu}$ respectively), scalar top quark ($\tilde{t}$) and scalar light quarks ($\tilde{q}$). The results of similar searches performed with the OPAL data at centre-of-mass energies up to 183 GeV have already been published [16].

Two different scenarios are probed. In the first scenario, the decays of sfermions via the lightest neutralino, $\tilde{\chi}_1^0$, are considered, where $\tilde{\chi}_1^0$ is treated as the LSP and assumed to decay via an R-parity violating interaction. These are denoted "indirect decays". SUSY cascade decays via particles other than the LSP are not considered; however, when calculating limits in the R-parity violating framework analogous to the CMSSM, these cascade decays are taken into account by assuming a zero efficiency for their detection. In the second scenario, "direct" decays of sparticles to Standard Model particles are investigated. In this case, the sparticle is assumed to be the LSP, such that R-parity conserving decay modes do not contribute.

In both the direct and indirect decay scenarios, it is assumed that only one of the 45 Yukawa couplings is significantly non-zero at a time. Moreover, only values of the λ-couplings (λ, $\lambda^{'}$, $\lambda^{''}$) larger than $\mathcal{O}(10^{-5})$ are relevant to this analysis. For smaller couplings, the lifetime of sparticles would be sufficiently long to produce a secondary decay vertex clearly detached from the primary vertex, or even outside the detector. These topologies have not been considered in this paper. Decays outside the detector have been treated in [17].

Results published by the other LEP Collaborations can be found in [18]. Results have also been obtained by the CDF and D0 Collaborations [19, 20] at the Tevatron and by the H1 and ZEUS Collaborations [21, 22] at HERA.

The production and R-parity violating decays of $\tilde{\ell}$, $\tilde{\nu}$ via λ and $\lambda^{'}$, $\tilde{t}$ via $\lambda^{'}$ and $\tilde{q}$ via $\lambda^{''}$ are described in Section 2, together with the possible signal topologies resulting from these processes. Short descriptions of the OPAL detector and of the data samples used are presented in Section 3. The signal and background Monte Carlo simulations used in the different analyses are described in Section 4. Sections 5 to 9 describe the specific analyses optimised to search for R-parity violating processes. The physics interpretation is given in Section 10 which presents cross-section limits and interpretations in the CMSSM. A summary is given in Section 11.

2   Sparticle production and decays

This section briefly describes the production and decay modes of different sfermion species. A detailed description of the various decay channels, decay widths and assumptions can be found in [16]. The decay modes studied, resulting from non-zero λ, $\lambda^{'}$ and $\lambda^{''}$ couplings, are presented in Table 1. Table 1 also summarises the production and decay mechanisms as well as the coupling involved in each decay and the final state topologies. In the indirect decays, the particles resulting from the $\tilde{\chi}_1^0$ decay are shown in parentheses. The sneutrino indirect $\lambda^{'}$ decays followed by $\tilde{\chi}_1^0 \rightarrow \ell q\bar{q}$, leading to topologies with jets and one or more leptons, are not investigated because the branching ratio into these final states is not significant. In the available phase space and for the CMSSM parameter space relevant to these analyses, the decay $\tilde{\chi}_1^0 \rightarrow \nu q\bar{q}$ is preferred with respect to the decay $\tilde{\chi}_1^0 \rightarrow \ell q\bar{q}$ because of the light sneutrino.

Production and Decay		Coupling	Topology	Section
$\tilde{\ell}^-\tilde{\ell}^+ \rightarrow$	$\nu\ell^- \bar{\nu}\ell^+$	λ direct	$2\,\ell + E_{miss}$	5.2
$\tilde{\nu}\bar{\tilde{\nu}} \rightarrow \nu\tilde{\chi}_1^0\, \bar{\nu}\tilde{\chi}_1^0 \rightarrow$	$\nu(\overset{(-)}{\nu}\ell^+\ell^-)\, \bar{\nu}(\overset{(-)}{\nu}\ell^+\ell^-)$	λ indirect	$4\,\ell + E_{miss}$	5.3
$\tilde{\nu}\bar{\tilde{\nu}} \rightarrow$	$\ell^-\ell^+\, \ell^+\ell^-$	λ direct	$4\,\ell$	5.3
$\tilde{\ell}^-\tilde{\ell}^+ \rightarrow \ell^-\tilde{\chi}_1^0\ell^+\tilde{\chi}_1^0 \rightarrow$	$\ell^-(\overset{(-)}{\nu}\ell^+\ell^-)\, \ell^+(\overset{(-)}{\nu}\ell^+\ell^-)$	λ indirect	$6\,\ell + E_{miss}$	5.4
$\tilde{t}_1\bar{\tilde{t}}_1 \rightarrow$	$e^+q\, e^-\bar{q}$	λ' direct	$2\,e + 2$ jets	6
$\tilde{t}_1\bar{\tilde{t}}_1 \rightarrow$	$\mu^+q\, \mu^-\bar{q}$	λ' direct	$2\,\mu + 2$ jets	6
$\tilde{t}_1\bar{\tilde{t}}_1 \rightarrow$	$\tau^+q\, \tau^-\bar{q}$	λ' direct	$2\,\tau + 2$ jets	6
$\tilde{\ell}^-\tilde{\ell}^+ \rightarrow \ell^-\tilde{\chi}_1^0\ell^+\tilde{\chi}_1^0 \rightarrow$	$\ell^-(\ell^\pm q\bar{q}')\, \ell^+(\ell^\pm q\bar{q}')$	λ' indirect	$\geq 2\ell +$ jets	7
	$\ell^-(\overset{(-)}{\nu}q\bar{q})\, \ell^+(\ell^\pm q\bar{q}')$	λ' indirect	$\geq 2\ell +$ jets	7
	$\ell^-(\overset{(-)}{\nu}q\bar{q})\, \ell^+(\overset{(-)}{\nu}q\bar{q})$	λ' indirect	$\geq 2\ell +$ jets	7
$\tilde{\nu}\bar{\tilde{\nu}} \rightarrow \nu\tilde{\chi}_1^0\, \bar{\nu}\tilde{\chi}_1^0 \rightarrow$	$\nu(\overset{(-)}{\nu}q\bar{q})\, \bar{\nu}(\overset{(-)}{\nu}q\bar{q})$	λ' indirect	4 jets $+ E_{miss}$	8
$\tilde{\nu}\bar{\tilde{\nu}} \rightarrow$	$q\bar{q}\, \bar{q}q$	λ' direct	4 jets	9
$\tilde{\ell}^-\tilde{\ell}^+ \rightarrow$	$\bar{q}q'\, q\bar{q}'$	λ' direct	4 jets	9
$\tilde{q}\bar{\tilde{q}} \rightarrow$	$\bar{q}\bar{q}'\, qq'$	λ'' direct	4 jets	9

Table 1: *List of production and decay mechanisms of the channels that are covered by the various analyses described in this paper. The couplings involved and decay type together with the resulting topologies are given in the second and third columns, respectively. The corresponding section number, where details of the relevant analysis are presented, is indicated in the last column.*

3 Data samples and OPAL detector

The analyses presented in this paper use the data collected at LEP from centre-of-mass energies ($\sqrt{s}$) between 189 GeV and 209 GeV, including the data obtained at the highest energies attained by LEP in the year 2000. The total data sample corresponds to an integrated luminosity of about 610 pb^{-1}. The data set collected at energies $\sqrt{s} \geq 206$ GeV has a luminosity weighted average centre-of-mass energy of 206.6 GeV. The results presented here are then combined with results obtained using data at lower energies [16]. The various integrated luminosities of the data taken between 1998 and 2000 are summarised in Table 2. The integrated luminosity is measured with a precision of 0.3−0.4% [23]. These uncertainties are taken into account in the limit calculation in all channels considered.

Year	1998	1999				2000	
$\sqrt{s}$ (GeV)	189	192	196	200	202	< 206	≥ 206
$\mathcal{L}$ (pb^{-1})	179	29	73	74	37	87	133

Table 2: *Integrated luminosities recorded with the OPAL detector between 1998 and 2000. Due to different requirements on the operation of the OPAL subdetectors the precise integrated luminosity differs from one analysis to another.*

A complete description of the OPAL detector can be found in Ref. [24], and only a brief overview is given here.

The central detector consisted of a system of tracking chambers providing charged particle tracking over the polar angle[2] range of $|\cos\theta| < 0.96$ inside a 0.435 T uniform magnetic field parallel to the beam axis. The central tracking system was composed of a large volume jet chamber containing a high precision drift chamber and a two-layer silicon microstrip vertex detector [25], and was surrounded by a set of z chambers measuring track coordinates along the beam direction. A lead-glass electromagnetic calorimeter located outside the magnet coil covered the full azimuthal range with excellent hermeticity in the polar angle range of $|\cos\theta| < 0.82$ in the barrel region and $0.81 < |\cos\theta| < 0.984$ in the endcap regions. The magnet return yoke was instrumented to comprise the barrel and the endcap sections of the hadron calorimeter. With the hadron pole tip detectors included, the hadron calorimeter covered the region with $|\cos\theta| < 0.99$. Four layers of muon chambers covered the outside of the hadron calorimeter. A system of forward detectors close to the beam axis completed the geometrical acceptance down to 24 mrad, except for the regions where a tungsten shield was present to protect the detectors from synchrotron radiation. The forward detectors included a lead-scintillator sandwich calorimeter, a ring of lead-scintillator modules, scintillating tile counters [26] and the silicon-tungsten luminometer [27] located on both sides, a few meters away from the interaction point.

The tracks and calorimeter clusters used in the analyses were required to satisfy minimum quality criteria. These were slightly different for the analysis of purely leptonic final states and for the analyses with jets, either with or without leptons. For leptonic final states, a track was

---

[2]The OPAL coordinate system is defined so that the z axis is in the direction of the electron beam, the x axis points towards the centre of the LEP ring, and θ and ϕ are the polar and azimuthal angles, defined relative to the $+z$ and $+x$ axes, respectively. The radial coordinate is denoted as r.

required to have at least 20 hits in the wire tracking chambers, the first of which was required to be at a radius of less than 75 cm, and to have a momentum transverse to the beam direction larger than 0.1 GeV. Its distance of closest approach to the interaction point in the transverse plane (d_0) had to be less than 1 cm and the distance along the beam direction less than 40 cm. Clusters of energy deposited in the barrel region of the electromagnetic calorimeter were taken into account in the analyses if their energy was larger than 0.1 GeV. Similarly, endcap electromagnetic energy clusters were taken into account in the analyses if their energy was larger than 0.2 GeV and if the cluster was composed of at least two adjacent lead blocks. Hadron calorimeter energy clusters had to contain an energy in excess of 0.6 MeV in the barrel and endcap regions, and 3 GeV in the pole tips. For leptons with jets and for purely hadronic channels, tracks in the central detector and energy clusters in the calorimeters were required to satisfy the quality criteria employed in [28].

In calculating the total visible energies and momenta of events and individual jets, corrections were applied to prevent double-counting of energy in the case of tracks and associated energy clusters. For the leptonic channels, an algorithm based on a global approach described in [29] was used. For jets with leptons and for purely hadronic channels, an algorithm matching tracks and calorimeter energy clusters, described in [28], was employed.

4   Monte Carlo simulation

Monte Carlo samples were generated corresponding to charged slepton, sneutrino, stop and squark pair-production processes as well as to Standard Model processes. All generated events were processed through the full simulation of the OPAL detector [30], and the same analysis chain was applied to simulated events as to the data.

All sparticle production and decays considered in this paper, except for stop production described below, were simulated at various centre-of-mass energies between 189 GeV and 209 GeV and for various sfermion masses between 45 and 103 GeV using the Monte Carlo program SUSYGEN [31]. All MC samples of signal events contain 1000 events per mass point.

Charged and neutral sleptons decaying via a λ coupling were simulated at $\sqrt{s} = 189$ and 205 GeV. Charged sleptons decaying indirectly via a $\lambda^{'}$ coupling were simulated at $\sqrt{s} = 183$ and 205 GeV. The selection efficiencies were interpolated (or extrapolated) for the centre-of-mass energies where no samples were generated. A few test samples were produced to test the validity of the interpolation.

For charged and neutral sleptons decaying directly via a $\lambda^{'}$ coupling, production was done at $\sqrt{s} = 189$, 196, 200 and 206 GeV. Squark pair-production samples were generated at $\sqrt{s} = 189$, 192, 196, 200, 202 and 206 GeV. In both cases, the signal samples with the closest $\sqrt{s}$ were used for the centre-of-mass energies where no samples were simulated.

For the indirect decays, events were produced with three sparticle masses ($m_{\tilde{f}}$) and the $\tilde{\chi}_1^0$ mass was fixed such that $\Delta m = m_{\tilde{f}} - m_{\tilde{\chi}_1^0} = m_{\tilde{f}}/2$. Samples were also simulated at the kinematic limit with $\Delta m = m_{\tilde{f}} - m_{\tilde{\chi}_1^0} = 5$ GeV to account for changes in the event topologies. The values of Δm were chosen to cover a wide range of event topologies for a limited number of Monte Carlo events. For charged sleptons decaying indirectly with a λ and a $\lambda^{'}$ coupling, selection efficiencies were also obtained using samples generated with Δm equal to the mass of the lepton plus 0.1 GeV in order to cover the small Δm region. To study the selection efficiency

dependency on large Δm, samples of sneutrinos decaying indirectly with a λ and a $\lambda^{'}$ coupling were also generated with $m_{\tilde{\chi}_1^0} = 10$, 25 and 40 GeV, respectively for $m_{\tilde{\nu}} < 50$ GeV, $70 < m_{\tilde{\nu}} < 80$ GeV and 90 GeV $< m_{\tilde{\nu}}$. For charged slepton indirect decays via $\lambda^{'}$, events were simulated for each lepton flavour corresponding to the first index of $\lambda^{'}$. The quark flavours corresponding to the second and third indices of $\lambda^{'}$ were fixed to the first and second generation, with the exception of a few additional samples containing bottom quarks for systematic checks. All possible sparticle pair-production processes were simulated only at 183 GeV [16] in order to determine the λ-like couplings which give the lowest and the highest selection efficiencies. At higher centre-of-mass energies, only the decays governed by these two couplings were simulated and considered when computing results.

Charged and neutral sleptons decaying directly via a $\lambda^{'}$ coupling were generated using the Lund string fragmentation scheme of PYTHIA [32, 33]. In this scheme, the final state quarks are evolved according to the "Lund Parton Shower" model. A colour string is formed between colour singlet $q\bar{q}$ states. The two quarks are subsequently evolved in time and space, emitting gluon radiation between the two quarks. The jets are relatively soft owing to the gluon radiation between the quark states. In the case of squark production, only the independent fragmentation model was implemented at the generator level. In this scheme, the final state quarks are treated as independent particles with respect to each other. There is no QCD radiation between the final state quarks, and the hadronization process produces relatively hard jets. For systematic studies additional smuon samples were generated by the independent fragmentation model.

For a stop decaying via the $\lambda^{'}$ coupling into a quark and a lepton, all nine combinations of quark and lepton flavours in the final state were generated at $\sqrt{s} = 189$, 192, 196, 200, 202 and 207 GeV. Since stop masses below 73 GeV were excluded in [16], only stop masses between 65 and 103 GeV were considered here. The production and decay of the stop were simulated as described in [34]. The stops were hadronised to form colourless hadrons using the Peterson fragmentation function [35], and associated fragmentation particles according to the Lund string fragmentation scheme. For the decay, a colour string was stretched between the spectator quark and the quark from the stop decay. Further hadronisation was also done using the Lund scheme. The left-right stop mixing angle, $\theta_{\tilde{t}}$, was set to zero. The dependences of the detection efficiencies on the fragmentation function, on the mixing angle and on the Fermi motion were evaluated by generating additional Monte Carlo samples with the appropriate parameters varied.

The main sources of background arise from Standard Model two-photon processes ($e^+e^- \rightarrow e^+e^-\gamma\gamma \rightarrow e^+e^-X$), and from four-fermion ($e^+e^- \rightarrow f\bar{f}f\bar{f}$) and two-fermion (lepton-pair $e^+e^- \rightarrow (Z/\gamma)^* \rightarrow l\bar{l}$ and multi-hadronic $e^+e^- \rightarrow (Z/\gamma)^* \rightarrow q\bar{q}$) final states. For two-photon processes, the PHOJET [36] and HERWIG [37] generators were used to simulate hadronic final states. The Vermaseren [38] generator was used to estimate the background contribution from all two-photon $e^+e^-\ell^+\ell^-$ final states. Four-fermion final states, other than two-photon events, were simulated with grc4f [39], which takes into account all interfering four-fermion diagrams with the exception of the multiperipheral two-photon processes. An $e^+e^-\ell^+\ell^-$ four-fermion sample generated with grc4f v2.2 with all interfering four-fermion diagrams including the multiperipheral two-photon processes was compared with the standard combination of grc4f v2.1 and Vermaseren events for a systematic cross-check. For final states with hadronic jets, systematic studies were performed using KORALW [40], which internally uses grc4f matrix elements. For purely hadronic final states, additional special samples generated with KandY [41], a special version of KORALW running concurrently with YFSWW3 [42], were also used. For the

9

two-fermion final states, BHWIDE [43] was used for the ee(γ) final state and KORALZ [44] and KK2F [45] for the $\mu\mu$ and the $\tau\tau$ states. The multi-hadronic events, qq(γ), were simulated using PYTHIA [32] and KK2F.

Final states with six or more primary fermions were not included in the background Monte Carlo samples but they are expected to make only a negligible contribution to the background.

5   Multi-lepton final states

This section describes the searches for purely leptonic final states resulting from pair-production of neutral or charged sleptons, with subsequent direct or indirect λ decays (see Table 1). The inefficiencies and systematic uncertainties associated with each analysis are estimated in a similar way for all multi-lepton final state searches, and are presented in Section 5.5. The selections of purely leptonic final states use the data collected at centre-of-mass energies between 189 GeV and 209 GeV corresponding to an integrated luminosity of 613.6 pb^{-1}.

5.1   Event and lepton selection

Multi-hadronic, cosmic and Bhabha scattering events were vetoed [46]. A loose high multiplicity veto was also applied: events were rejected if the total multiplicity of tracks in the central detector and energy clusters in the electromagnetic calorimeters satisfying the quality criteria described in Section 3 was greater than 26. At the preselection level, it was also required that the ratio of the number of such "good" tracks as defined in Section 3 to the total number of reconstructed tracks be greater than 0.2 in order to reduce backgrounds from beam-gas and beam-wall events. At least two good tracks were required.

Only tracks with $|\cos\theta| < 0.95$ were considered for lepton identification. Tracks resulting from photon conversion were rejected using the algorithm described in [47]. A track was considered "isolated" if the total energy of other charged particle tracks within 10° of the lepton candidate was less than 2 GeV. In these searches, a very loose lepton identification is sufficient. A track was selected as an electron candidate if one of the following three criteria was satisfied: *(i)* the output probability of the neural net algorithm described in [48] was larger than 0.8; *(ii)* the electron selection algorithm described in [49] for the barrel region or in [50] for the endcap region was satisfied; *(iii)* $0.5 < E/p < 2.0$, where p is the momentum of the electron candidate and E is the energy of the electromagnetic calorimeter energy cluster associated with the track. The simple criterion *(iii)* identifies most electrons. The algorithms *(i)* and *(ii)* are based predominantly on E/p, dE/dx and shower shape information, and are used to increase the electron selection efficiency. These algorithms are also used in the lepton plus jets analyses. A track was selected as a muon candidate according to the criteria employed in OPAL's analysis of Standard Model muon pairs [51], that is, the track had associated activity in the muon chambers or hadron calorimeters or it had a high momentum but was associated with only a small amount of energy deposited in the electromagnetic calorimeter. Identified electrons or muons were also considered as tau candidates. Taus were selected by requiring that there be at most three tracks within a 35° cone. The invariant mass computed using all good tracks and electromagnetic energy clusters within the above cone had to be less than 3 GeV. For muon and electron candidates, the momentum was estimated from the charged particle track momentum measured in the central detector, while for tau candidates, the momentum

was estimated from the vector sum of the measured momenta of the charged particle tracks within the tau cone.

For the two- and six-lepton final states, the large background from two-photon processes was reduced by requiring that the measured amount of energy deposited in each silicon tungsten calorimeter, in each forward calorimeter, and in each side of the gamma-catcher be less than 5 GeV ("forward detector vetoes").

5.2 Final states with two leptons and missing energy

Final states with two charged leptons and missing energy may result from direct charged slepton decays via a λ coupling. The analysis was optimised to retain good signal efficiency while reducing the background, mainly due to $W^+W^- \longrightarrow \ell^+\nu\ell^-\nu$ events and two-photon processes.

The following criteria were applied in addition to those described in Section 5.1.

(1) Events had to contain exactly two identified and oppositely-charged leptons, each with a transverse momentum with respect to the beam axis greater than 2 GeV.

(2) The background from two-photon processes and "radiative return" events ($e^+e^- \to Z\gamma$, where the γ escapes down the beam pipe) was reduced by requiring that the polar angle of the missing momentum, θ_{miss}, satisfy $|\cos\theta_{\text{miss}}| < 0.9$.

(3) To reduce further the residual background from Standard Model lepton pair events, it was required that $m_{\text{vis}}/\sqrt{s} < 0.80$, where m_{vis} is the invariant mass derived from the measured energy and momentum of all the tracks and electromagnetic energy clusters observed in the event, hereafter referred to as event visible mass.

(4) The acoplanarity angle[3] (ϕ_{acop}) between the two leptons was required to be greater than $10°$ in order to reject Standard Model leptonic events, and smaller than $175°$ in order to reduce the background due to photon conversions. The acoplanarity angle distribution is shown in Figure 1 after cuts (1) to (3). Figure 1 demonstrates the good discriminating power of this quantity. There is a disagreement between data and Standard Model expectation which is characteristic of the presence in the data of un-modelled two-photon events with low acoplanarity. The acollinearity angle[4] (θ_{acol}) was also required to be greater than $10°$ and smaller than $175°$.

(5) It was required that there be no electromagnetic energy cluster with an energy larger than 25 GeV and no associated track and no hadronic energy cluster with an energy larger than 10 GeV and no associated track.

(6) In order to reduce the background from two-photon events with high transverse momentum, complementary cuts were applied for different regions of acoplanarity. For events with small acoplanarity ($\phi_{\text{acop}} < 1.2$ rad), a cut was made on a_t^{miss}, the component of the missing momentum vector perpendicular to the event thrust axis in the plane transverse

---

[3]The acoplanarity angle, ϕ_{acop}, is defined as $180°$ minus the angle between the two lepton momentum vectors projected into the $x - y$ plane.

[4]The acollinearity angle, θ_{acol}, is defined as $180°$ minus the 3-dimensional space-angle between the two lepton momentum vectors.
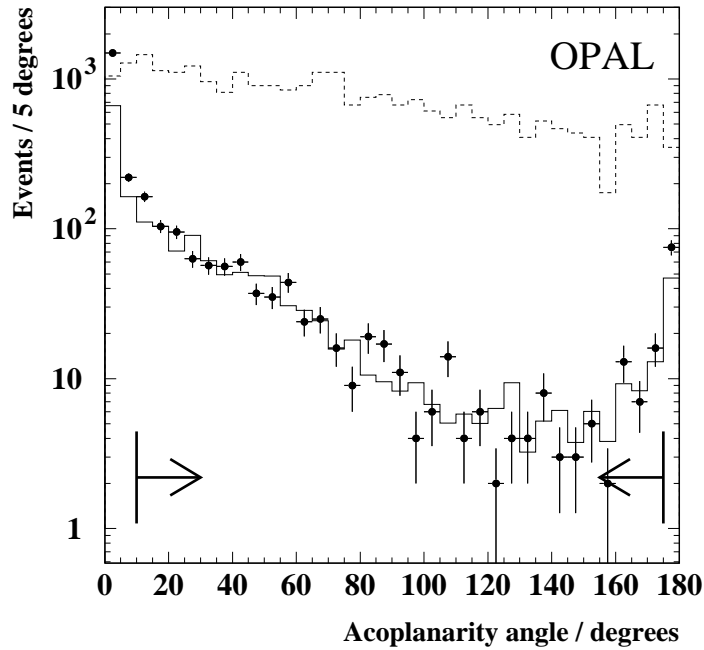
Figure 1: *Final states with two leptons and missing energy: distribution of the acoplanarity angle after applying cuts (1) to (3). The dashed histogram shows signal Monte Carlo events for direct decays of $\tilde{e}$ via λ_{122} with $m_{\tilde{e}} = 78$ GeV. Data are shown as points and the sum of all Monte Carlo background processes is shown as a solid line. Data used for this plot were collected in the year 2000 at a luminosity weighted average centre-of-mass energy of 206.6 GeV. The simulated signal events have arbitrary normalisation. The arrows point into the region accepted by the cuts. The disagreement between data and Standard Model expectation, visible in a few bins, is due to the presence of un-modelled two-photon events in the data.*

to the beam axis. For events with large acoplanarity ($\phi_{\mathrm{acop}} > 1.2$ rad), a cut was made on p_t^{miss}, the missing transverse momentum. In the low acoplanarity region, a_t^{miss} provides a good discriminating power since it is less sensitive than p_t^{miss} to the presence of neutrinos from tau decays or poorly measured tracks. However, in the large acoplanarity region, a_t^{miss} does not discriminate sufficiently between signal and background and p_t^{miss} is used. A further subdivision was applied according to the event visible energy, E_{vis}, which is defined as the scalar sum of the energy of all tracks and electromagnetic energy clusters of the event. This selection provides a good discrimination between events with genuine missing energy and events which have missing energy due to secondary decays such as τ decays. It is optimized to retain good signal efficiency also in the case of very small visible energy:

1. Cuts in the small acoplanarity region:
   (a) If $E_{\mathrm{vis}}/\sqrt{s} < 0.06$, then $a_t^{\mathrm{miss}}/\sqrt{s} > 0.015$,
   (b) If $E_{\mathrm{vis}}/\sqrt{s} > 0.06$, then $a_t^{\mathrm{miss}}/\sqrt{s} > 0.0175$.

2. Cuts in the large acoplanarity region:
   (a) If $E_{\mathrm{vis}}/\sqrt{s} < 0.06$, then $p_t^{\mathrm{miss}}/\sqrt{s} > 0.025$,
   (b) If $E_{\mathrm{vis}}/\sqrt{s} > 0.06$, then $p_t^{\mathrm{miss}}/\sqrt{s} > 0.035$.
   (c) The event transverse momentum computed without the hadron calorimeter was required to be larger than $0.02 \times \sqrt{s}$. This cut rejects events with a large measured transverse momentum due to fluctuations in the hadron calorimeter.

(7) The background from two-photon processes and $\mathrm{W^+W^-}$ production was further reduced by categorising the events in different classes according to the flavour of the leptons in the final state. The flavours of the two identified leptons were required to match the flavours of the leptons expected for each signal class. Events were selected by applying cuts on the momentum of the two leptons and on the visible energy:

- $e\nu e\nu$ selection: $E_{\mathrm{vis}}/\sqrt{s} < 0.8$ and $p_{\mathrm{max}}/E_{\mathrm{beam}} > 0.1$, where p_{max} is the momentum of the most energetic electron and E_{beam} is the beam energy.
- $\mu\nu\mu\nu$ selection: $E_{\mathrm{vis}}/\sqrt{s} < 0.7$, $0.05 < p_{\mathrm{min}}/E_{\mathrm{beam}} < 0.60$ and $0.05 < p_{\mathrm{max}}/E_{\mathrm{beam}} < 0.95$, where p_{min} is the momentum of the less energetic muon and p_{max} is the momentum of the most energetic muon.
- $\tau\nu\tau\nu$ selection: $E_{\mathrm{vis}}/\sqrt{s} < 0.4$, $p_{\mathrm{min}}/E_{\mathrm{beam}} < 0.30$ and $0.04 < p_{\mathrm{max}}/E_{\mathrm{beam}} < 0.5$.
- $e\nu\mu\nu$ selection: $0.12 < E_{\mathrm{vis}}/\sqrt{s} < 0.8$ and $p_{\mathrm{max}}/E_{\mathrm{beam}} > 0.15$.
- $e\nu\tau\nu$ selection: $p_{\mathrm{min}}/E_{\mathrm{beam}} < 0.5$ and $p_{\mathrm{max}}/E_{\mathrm{beam}} > 0.1$.
- $\mu\nu\tau\nu$ selection: $p_{\mathrm{min}}/E_{\mathrm{beam}} < 0.5$ and $p_{\mathrm{max}}/E_{\mathrm{beam}} > 0.1$.

Table 3 shows the results for the different selections at centre-of-mass energies from 189 GeV to 209 GeV. Since the detection efficiencies are independent of the charged slepton species within the statistical uncertainties, results are quoted irrespective of the charged slepton species but only for the different possible final states. The lowest efficiencies arise from final states with two taus and missing energy and the highest ones from final states with two muons and missing energy. They range from 18% ($\tau\nu\tau\nu$) to 66% ($\mu\nu\mu\nu$) for charged slepton masses between 45 and 103 GeV. The main contribution to the background comes from four-fermion processes which, depending on the final state lepton flavours, account for $90-100\%$ of the Standard Model expectation.

Physics process	Eff. (%)	Data	Tot. bkg MC	Data > 206 GeV	MC > 206 GeV
$\tilde{\ell}^+\tilde{\ell}^- \rightarrow$					
$e\nu e\nu$	$54 - 64$	135	$145.3 \pm 0.9 \pm 10.7$	31	$28.6 \pm 0.1 \pm 3.0$
$\mu\nu\mu\nu$	$48 - 66$	99	$101.8 \pm 0.6 \pm 11.1$	22	$21.9 \pm 0.1 \pm 3.3$
$\tau\nu\tau\nu$	$18 - 27$	166	$161.5 \pm 2.2 \pm 22.0$	25	$35.6 \pm 0.6 \pm 6.7$
$e\nu\mu\nu$	$55 - 64$	463	$502.4 \pm 2.0 \pm 37.1$	94	$106.2 \pm 0.3 \pm 10.5$
$e\nu\tau\nu$	$37 - 44$	429	$459.9 \pm 2.7 \pm 39.7$	85	$98.0 \pm 0.7 \pm 11.4$
$\mu\nu\tau\nu$	$38 - 47$	434	$451.0 \pm 2.7 \pm 41.0$	84	$97.4 \pm 0.7 \pm 11.9$

Table 3: *Final states with two leptons and missing energy for $\sqrt{s} = 189 - 209$ GeV and for $\sqrt{s} > 206$ GeV: signal selection efficiencies, observed numbers of events in the data and background estimates from Standard Model processes. The first uncertainty on the background estimate is statistical and the second is systematic.*

5.3 Final states with four leptons, with or without missing energy

Final states with four charged leptons and no missing energy may result from direct sneutrino decays via a λ coupling while final states with missing energy may result from indirect sneutrino decays via a λ coupling. Two analyses have been developed and optimised separately for these two final states.

The following criteria were applied to select a possible signal with four leptons and missing energy:

(1) The scaled event total momentum was required to be $p_{\mathrm{vis}}/\sqrt{s} > 0.035$ and the direction of the event missing momentum was required to satisfy $|\cos\theta_{\mathrm{miss}}| < 0.9$.

(2) Events were required to have between three and eight tracks, each with a transverse momentum relative to the beam axis greater than 1.5 GeV.

(3) Events had to contain at least three identified leptons, each with a transverse momentum relative to the beam axis greater than 1.5 GeV.

(4) It was also required that $E_{\mathrm{vis}}/\sqrt{s} < 0.9$.

(5) The total leptonic energy, defined as the sum of the energies of all identified leptons, was required to be greater than $0.65 \times E_{\mathrm{vis}}$.

(6) It was required that the scaled longitudinal component of the event momentum satisfy $p_{\mathrm{vis,z}}/\sqrt{s} < 0.25$.

Table 4 shows the results for the selections with the highest and the lowest efficiencies at centre-of-mass energies from 189 GeV to 209 GeV. Efficiencies are quoted for $\Delta m \leq m_{\tilde{\nu}}/2$. Since the detection efficiencies are independent of the sneutrino species within the statistical uncertainties, results are quoted irrespective of the sneutrino species. These analyses do not differentiate the different lepton flavours present in the final states and the number of observed events in the data and the background estimates are therefore the same for the various signal

Physics process	Eff. (%)	Data	Tot. bkg MC	Data > 206 GeV	MC > 206 GeV
$\tilde{\nu}\tilde{\nu} \rightarrow$ $\mu\mu\nu\nu\mu\mu\nu\nu$ $\tau\tau\nu\nu\tau\tau\nu\nu$	$72 - 83$ $13 - 28$	16	$15.6 \pm 0.3 \pm 2.5$	4	$4.8 \pm 0.1 \pm 0.7$

Table 4: *Final states with four leptons and missing energy for $\sqrt{s}$ = 189 - 209 GeV and separately for $\sqrt{s} > 206$ GeV: signal selection efficiencies for $\Delta m \leq m_{\tilde{\nu}}/2$, observed number of events in the data and background estimates from Standard Model processes. The uncertainties on the background estimates are the quadratic sum of the statistical and systematic uncertainties. Many more final states have been studied; only the final states with the highest and lowest efficiencies are reported here.*

final states. However, the signal detection efficiencies depend strongly on the charged lepton flavours present in the final states. The lowest efficiencies arise from final states with four taus and missing energy and the highest ones from final states with four muons and missing energy. They range from 13% ($\tau\tau\nu\nu\tau\tau\nu\nu$) to 83% ($\mu\mu\nu\nu\mu\mu\nu\nu$) for a sneutrino mass between 45 and 103 GeV and $\Delta m \leq m_{\tilde{\nu}}/2$. As the value of Δm is increased above $m_{\tilde{\nu}}/2$, the selection efficiencies drop by a factor 2 to 3, depending on $m_{\tilde{\nu}}$ and Δm, due to the larger fraction of missing energy and lower energy of the charged leptons in the final state. The main contribution to the background comes from four-fermion processes, which account for about 75% of the Standard Model expectation. The remaining 25% arises from processes yielding two-lepton final states.

To select final states without missing energy, the following requirements were imposed:

(1) Events were required to have at least three tracks with a transverse momentum relative to the beam axis greater than 1.0 GeV.

(2) Events had to have between three and ten identified leptons, each with a transverse momentum relative to the beam axis greater than 1.5 GeV.

(3) It was required that $E_{\mathrm{vis}}/\sqrt{s} > 0.9$.

(4) To eliminate events containing photons, events were required not to have electromagnetic energy clusters with energies greater than 10 GeV not associated to a track.

(5) The total leptonic energy was required to be greater than $0.7 \times E_{\mathrm{vis}}$.

(6) To reduce the residual four-fermion background, pairs were formed with the four most energetic particle tracks, and the invariant mass was computed for each pair. Events were selected if one of the three possible pairings satisfied $|m_{i,j} - m_{k,l}|/(m_{i,j} + m_{k,l}) < 0.4$, where $m_{i,j}$ is the invariant mass of the pair (i, j). Only pairs with invariant mass $m_{i,j}$ greater than 20 GeV were used in the computation.

To maximise the detection efficiencies for final states without missing energy, especially for the four tau final states which contain missing energy from the neutrinos present in the tau decays, this analysis was combined with the analysis for final states with missing energy, previously described. Events passing either set of criteria were accepted as candidates for the pair-production of sneutrinos followed by a direct decay. Table 5 shows the results for the

Physics process	Eff. (%)	Data	Tot. bkg MC	Data > 206 GeV	MC > 206 GeV
$\widetilde{\nu}\widetilde{\nu} \rightarrow$					
$\mu\mu\mu\mu$	$75 - 81$				
		42	$32.0 \pm 0.3 \pm 3.2$	8	$6.7 \pm 0.1 \pm 0.9$
$\tau\tau\tau\tau$	$32 - 36$				

Table 5: *Final states with four leptons and no missing energy (including candidates from the analysis for four leptons with missing energy) for $\sqrt{s} = 189$ - 209 GeV and for $\sqrt{s} > 206$ GeV: signal selection efficiencies, observed number of events in the data and background estimates from Standard Model processes. The uncertainties on the background estimates are the quadratic sum of the statistical and systematic uncertainties. Many more final states have been studied; only the final states with the highest and lowest efficiencies are given in the table.*

selections with the highest and the lowest efficiencies at centre-of-mass energies from 189 GeV to 209 GeV. The lowest efficiencies arise for final states with four taus and the highest ones from final states with four muons. They range from 32% ($\tau\tau\tau\tau$) to 81% ($\mu\mu\mu\mu$) for a sneutrino mass between 45 and 103 GeV. The main contribution to the background comes from four-fermion processes, which account for about 80% of the Standard Model expectation. The remaining 20% arise from processes yielding two-lepton final states.

5.4 Final states with six leptons and missing energy

Events with six charged leptons and missing energy in the final state may result for example from indirect charged slepton decays with a λ coupling. Here, the strategy adopted was to design two complementary searches for events with six leptons either with or without missing energy. Events satisfying either selection were accepted, which improved the detection efficiencies compared to only allowing events with significant missing energy.

The following criteria were applied for the selection of final states with six leptons and missing energy:

(1) The direction of the event missing momentum was required to satisfy $|\cos\theta_{\mathrm{miss}}| < 0.9$.

(2) The scaled event total momentum was required to be $p_{\mathrm{vis}}/\sqrt{s} > 0.035$.

(3) To reduce the background from two-photon processes and di-lepton final states, it was required that $0.2 < E_{\mathrm{vis}}/\sqrt{s} < 1.0$.

(4) Events were required to have at least three tracks with a transverse momentum relative to the beam axis greater than 0.3 GeV. Tracks originating from photon conversions were excluded from this analysis.

(5) Events had to contain between four and ten identified leptons, at least two of them with a transverse momentum relative to the beam axis greater than 1.5 GeV, and the third one with a transverse momentum relative to the beam axis greater than 0.3 GeV.

(6) The total leptonic energy was required to be greater than $0.55 \times E_{\mathrm{vis}}$.

These criteria were used for the search for final states with six leptons without missing energy:

(1) To reduce the background from two-photon processes and di-lepton final states, it was required that $0.2 < E_{\text{vis}}/\sqrt{s} < 1.2$.

(2) Events were required to have at least five tracks with a transverse momentum with respect to the beam axis greater than 1.0 GeV. Tracks from photon conversions were excluded.

(3) Events had to contain between four and twelve identified leptons, each with a transverse momentum with respect to the beam axis greater than 1.5 GeV.

(4) The total leptonic energy was required to be greater than $0.40 \times E_{\text{vis}}$.

Physics process	Eff. (%)	Data	Tot. bkg MC	Data > 206 GeV	MC > 206 GeV
$\tilde{\ell}^+\tilde{\ell}^- \rightarrow$					
$e\tau\tau\nu e\tau\tau\nu$	$38 - 63$				
$e\mu\mu\nu e\mu\mu\nu$	$78 - 92$				
$\mu\tau\tau\nu\mu\tau\tau\nu$	$59 - 69$	9	$8.5 \pm 0.2 \pm 1.3$	1	$1.5 \pm 0.04 \pm 0.3$
$\mu\mu\mu\nu\mu\mu\mu\nu$	$90 - 96$				
$\tau\tau\tau\nu\tau\tau\tau\nu$	$24 - 41$				
$\tau\mu\mu\nu\tau\mu\mu\nu$	$79 - 89$				

Table 6: *Final states with six leptons and missing energy for $\sqrt{s}$ = 189 - 209 GeV and for $\sqrt{s}$ > 206 GeV: signal selection efficiencies, observed number of events in the data and background estimates from Standard Model processes. The uncertainties on the background estimates are the quadratic sum of the statistical and systematic uncertainties.*

Table 6 shows the results for the events passing either selection at centre-of-mass energies from 189 GeV to 209 GeV. Since the detection efficiencies are independent of the charged slepton species within the statistical uncertainties, results are quoted irrespective of the charged slepton species. These analyses do not differentiate the different lepton flavours present in the final states and the number of observed events in the data and the background estimates are therefore the same for the various signal final states. However, the signal detection efficiencies depend strongly on the charged lepton flavours present in the final states. The lowest efficiencies arise from final states with six taus and missing energy and the highest ones from final states with six muons and missing energy. They range from 24% ($\tau\tau\tau\nu\tau\tau\tau\nu$) to 96% ($\mu\mu\mu\nu\mu\mu\mu\nu$) for a charged slepton mass between 45 and 103 GeV. The background is entirely due to four-fermion processes.

In the small Δm region, the final state charged leptons resulting from the charged slepton decay into a charged lepton and a neutralino may not be detected due to the small phase space available. In this case, the analysis searching for four leptons and missing energy is applied to maximise the detection efficiencies. The lowest efficiencies in the $\Delta m < 5$ GeV range were used. Signal selection efficiencies are of the order of 12-14%, depending on the charged slepton flavour. A total of 16 events was observed in the data and a background of $15.6 \pm 0.3 \pm 2.5$ was estimated from Standard Model processes for $\sqrt{s}$ = 189 - 209 GeV. For $\sqrt{s}$ > 206 GeV, the numbers are respectively 4 (data) and $4.8 \pm 0.1 \pm 0.7$ (background). The uncertainty quoted on the background estimate is the quadratic sum of the statistical and systematic uncertainties.

5.5 Inefficiencies and systematic uncertainties for leptonic final states

The inefficiency due to false forward detector vetoes, described in Section 5.1, caused by beam-related backgrounds or detector noise was estimated to range from 1.4 to 2.8%, depending on the data samples, from a study of randomly triggered beam crossings. The quoted efficiencies and background expectations take this effect into account.

The following systematic uncertainties on the signal detection efficiencies were considered:

1. The statistical uncertainty on the determination of the efficiency from the Monte Carlo simulation.

2. The systematic uncertainty on the integrated luminosity (0.3-0.4%).

3. The uncertainty due to the interpolation of the efficiencies (4.0%).

4. The lepton identification uncertainty (2.4% for the muons, 3.9% for the electrons and 4.7% for the taus).

5. The systematic uncertainty arising from the modelling of the variables used in the selections. This was estimated by recalculating the detection efficiencies using a new cut value shifted from its original value by a ratio of the means of the cut variable distributions of the data and of the Standard Model samples. The difference between the original efficiency and the new efficiency, usually less than 5%, is taken as systematic uncertainty due to the modelling of a cut variable.

The systematic uncertainty due to the trigger efficiency is negligible because of the high lepton transverse momentum requirement.

All cut variables are treated as independent; hence, systematic uncertainties originating from each variable are added in quadrature. The total systematic uncertainty was calculated by summing in quadrature the individual uncertainties.

Channel	$\sigma_\epsilon^{\mathrm{stat}}$ (%)	$\sigma_\epsilon^{\mathrm{sys}}$ (%)	$\sigma_{\mathrm{N_{bkg}}}^{\mathrm{tot}}$ (%)
$2\,\ell + E_{\mathrm{miss}}$	$2.2 - 6.7$	$4.3 - 31.2$	$7.4 - 18.9$
$4\,\ell + E_{\mathrm{miss}}$	$1.5 - 8.3$	$7.6 - 52.7$	$13.7 - 17.6$
$4\,\ell + E_{\mathrm{miss}}$ OR $4\,\ell$	$1.5 - 4.6$	$7.7 - 20.1$	$7.0 - 12.7$
$6\,\ell + E_{\mathrm{miss}}$ OR $6\,\ell$	$0.7 - 5.6$	$6.5 - 27.8$	$12.2 - 31.8$

Table 7: *Relative statistical and systematic uncertainties on the selection efficiency, $\sigma_\epsilon^{\mathrm{stat}}$ and $\sigma_\epsilon^{\mathrm{sys}}$, and relative total uncertainty on the number of expected Standard Model background events, $\sigma_{\mathrm{N_{bkg}}}^{\mathrm{tot}}$, for the various multi-lepton final state searches.*

The systematic uncertainty on the number of expected Standard Model background events is estimated in a similar way. The statistical uncertainty on this number is small, typically less than 1%, due to the large size of the Standard Model event samples. For final states with more than two leptons, an additional systematic uncertainty on the number of expected background events, arising from the imperfect simulation of four-fermion processes is taken into

account. It is determined by comparing predictions of grc4f version 2.2 including all interfering four-fermion diagrams to the default Monte Carlo predictions, which use Vermaseren for the two-photon processes and grc4f version 2.1 for the other four-fermion processes, and neglect the interference between the two. This systematic uncertainty ranges from 10 to 17%, depending on the analysis.

The relative statistical and systematic uncertainties on the selection efficiency, $\sigma_\epsilon^{\text{stat}}$ and $\sigma_\epsilon^{\text{sys}}$, and the relative total uncertainty on the number of expected Standard Model background events, $\sigma_{N_{\text{bkg}}}^{\text{tot}}$, are summarised in Table 7 for the multi-lepton final state searches presented in the previous sections.

6 Final states with two jets and two leptons

This section describes the selection for final states with two charged leptons, two jets and no missing energy. These final states may result from the direct decay of pair-produced stops via a λ' coupling. In contrast to the purely leptonic final states described in the previous section, the topologies searched for in this analysis involve hadronic jets; more stringent cuts are needed to obtain a purer lepton sample. Particles are considered as electrons or muons if they are either identified by the selection algorithms described in [49] and [50], or by an algorithm used for selecting semileptonic W decays, as described in [52]. A Neural Net (NN) based on track properties [53] is used to identify taus. Events were preselected by requiring the following criteria to be satisfied (the same criteria were also used for the analysis presented in Section 7):

The ratio of good tracks satisfying the criteria of Section 3 to the total number of reconstructed tracks had to be greater than 0.2 to reduce beam-gas and beam-wall background events. Events with fewer than eight good tracks were not considered, in order to reduce the background from Bhabha scattering. Events had to contain at least one identified electron or muon with a momentum p greater than 3 GeV, to reduce the background from final states with low energy leptons (electron or muon) arising for instance from semi-leptonic quark decays or misidentified particles. To reduce background from two-photon processes, it was required that the visible energy normalised to the centre-of-mass energy $E_{\text{vis}}/\sqrt{s}$ be greater than 0.3.

The following cuts were then applied:

(1) The visible energy had to be close to the centre-of-mass energy, i.e. $0.75 < E_{\text{vis}}/\sqrt{s} < 1.25$ for electron and muon and $0.5 < E_{\text{vis}}/\sqrt{s} < 1.0$ for tau final states.

(2) It was required that four jets be reconstructed using the Durham [54] algorithm, with $y_{34} > 0.001$, where y_{34} is the jet resolution at which the number of jets changes from 3 to 4. Both hadronic and leptonic objects are used in the jet reconstruction.

(3) Events had to contain at least one pair of identified oppositely-charged lepton candidates of the same flavour.

(4) To make use of the signal topology of two leptons and two jets, where a lepton and a jet stem from the same object, a five-constraint (5C) kinematic fit was performed for the two possible combinations of each lepton with each jet. The kinematic constraints are: the vector sum of all momenta has to be equal to zero, the total energy of all objects has to be equal to the centre-of-mass energy and the masses of the two reconstructed particles

have to be equal. From the three most energetic leptons of the same flavour, the two most isolated[5] were selected and the rest of the event was reconstructed as two jets. The combination with the highest fit probability was selected. The probability for the fit, based on the χ^2, was required to be larger than 0.01.

(5) The scaled momenta $p/\sqrt{s}$ of the most and second most energetic leptons had to be greater than 0.082 and 0.055, respectively, for final states with electrons and muons and greater than 0.055 and 0.0275, respectively, for taus.

(6) It was required that there be no track within a cone of half opening angle of 15° around the most energetic lepton candidate.

Figure 2 shows the distribution of the reconstructed stop mass after cut (6). The kinematic fit achieves a very good mass resolution. For stop masses above 75 GeV, the mass resolution is better than 0.8 GeV for final states containing either electrons or muons and better than 1.3 GeV for final states with taus. Events are counted only in a two sigma mass window around the mean reconstructed stop mass. For masses near the kinematic limit the mass resolution approaches zero. If the mass resolution is below 0.5 GeV, it is set to 0.5 GeV.
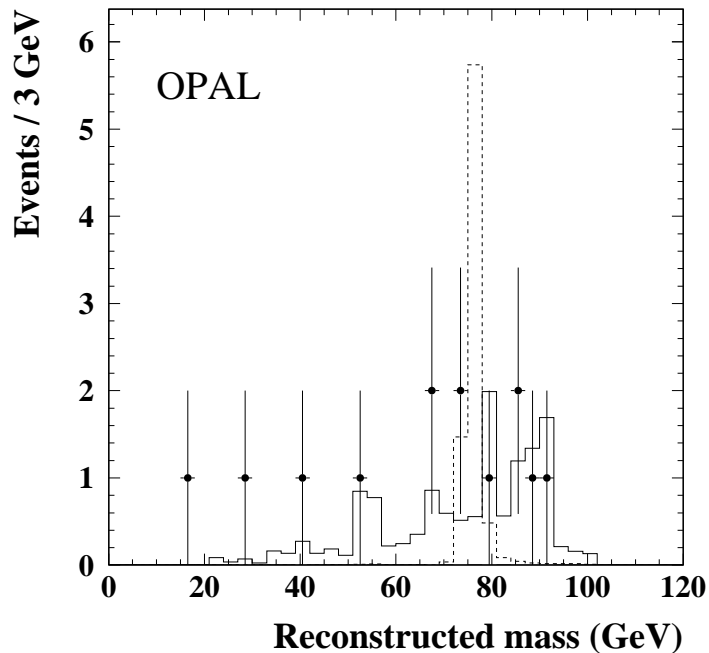
Figure 2: *Final states with two jets and two leptons: distribution of the reconstructed stop mass after cut (6) for the direct decay of stops into final states with two jets and two electrons. The signal is shown as the dashed line for a stop mass of 75 GeV. Data are shown as points and the sum of all Monte Carlo background processes is shown as a solid line. Data used for this plot were collected at centre-of-mass energies of 189–209 GeV. The simulated signal events have arbitrary normalisation. Uncertainties are statistical only.*

---

[5]The most isolated lepton is the one with the largest angle to the closest other track.

These cuts, including the cut of the two sigma mass window, yield an efficiency of more than 46% for a stop mass above 75 GeV for final states with either electrons or muons. For final states with taus, efficiencies above 15 % are reached for stop masses above 75 GeV. Table 8 shows the efficiencies, the number of candidate events observed in the data and the number of background events for the selection at centre-of-mass energies from 189 GeV to 209 GeV, corresponding to an integrated luminosity of 599.6 pb^{-1}. The main contribution to the background comes from four-fermion processes which amount to 100% of the Standard Model expectation for final states with muons and to 75−95% for final states with taus. In the electron channel, four-fermion events account for 45−75% of the Standard Model background, two-fermion processes contribute less than 5% and the remaining events are expected from two-photon interactions.

Physics process	Eff. (%)	Data	Tot. bkg MC	Data > 206 GeV	MC > 206 GeV
$\tilde{\bar{t}}\tilde{t} \rightarrow$					
2 jets $+ e^+ + e^-$	$46 - 55$	13	$13.8 \pm 1.4 \pm 1.2$	3	$3.3 \pm 0.5 \pm 0.3$
2 jets $+ \mu^+ + \mu^-$	$47 - 55$	7	$7.1 \pm 0.4 \pm 1.5$	0	$1.5 \pm 0.2 \pm 0.1$
2 jets $+ \tau^+ + \tau^-$	$15 - 25$	30	$34.4 \pm 1.0 \pm 4.1$	7	$7.9 \pm 0.6 \pm 0.9$

Table 8: *Final states with two jets and two leptons for $\sqrt{s}$ = 189 - 209 GeV and for $\sqrt{s} >$ 206 GeV: signal selection efficiencies, observed number of events in the data and background estimates from Standard Model processes. The first uncertainty on the background estimate is statistical and the second is systematic. The efficiencies are given for stop masses greater than 75 GeV for the signal at $\sqrt{s}$ = 207 GeV.*

Systematic uncertainties

The following systematic uncertainties on the signal efficiencies were considered:

1. The statistical uncertainties from the limited size of the Monte Carlo samples.

2. The systematic uncertainties on the integrated luminosity (0.3 - 0.4%).

3. The uncertainty due to the interpolation of efficiencies for mass values between the generated stop masses (less than 3%).

4. For the lepton identification, the highest uncertainty (4% for electrons) was taken for all flavours.

5. The systematic uncertainty arising from the modelling of the variables used in the selection, as described below.

6. The fragmentation of the stop was simulated using the fragmentation function from Peterson *et al.* with the ϵ parameter extrapolated from measurements of charm and bottom [55]. To check the model dependence of the fragmentation, it was also performed using the function from Bowler [56]. No significant change in the efficiency due to the difference in the fragmentation function was found. The difference was at most 0.5%, where a variation of the ϵ parameter of the $\tilde{t}$ in the Peterson *et al.* scheme was included. This uncertainty on $\epsilon_{\tilde{t}}$ was propagated from the uncertainty of ϵ_b and the uncertainty on the b-quark mass as described in detail in Ref. [55].

21

7. The signal events were produced for a zero mixing angle between the two stop eigenstates. The mixing angle describes the coupling between the stop and the Z^0, and therefore the energy distribution of the initial state radiation depends on this mixing angle. To check the dependence of the detection efficiency on this angle, events were generated with $\theta_{\tilde{t}} = 0.98$ rad, where the stop decouples from the Z^0. The change in efficiency was less than 0.5% for the two extreme cases.

8. The Fermi motion of the spectator quark in the stop-hadron influences its measured mass. The Fermi motion was increased from 220 MeV to 520 MeV and the efficiency changes by no more than 1%, which was taken as a systematic uncertainty.

The systematic uncertainty due to the uncertainty in the trigger efficiency was estimated to be negligible, because of the requirement of at least eight good tracks.

All of the above contributions to the systematic uncertainties result in a total systematic uncertainty of less than 7%.

The uncertainty in the signal efficiency and in the number of background events due to the modelling of the selection variables was estimated in the following way. First the mean and the r.m.s. of the distribution of the variable (y) was determined for the data and the Standard Model background simulation (SM MC). Then for each MC event (both signal and background) the variable was transformed as

$$y' = (y - \text{mean(SM MC)}) \cdot \text{r.m.s.(data)} / \text{r.m.s.(SM MC)} + \text{mean(data)}$$

The standard analysis was applied to signal and Standard Model background events with all variables transformed; the difference in the MC expectation due to the transformation was considered as the systematic uncertainty. The contributions for the different variables were added in quadrature.

The systematic uncertainty on the expected number of background events estimated in this way was found to be less than 20%, the largest contribution ($\sim 15\%$) stemming from the variable y_{34}. In addition, the difference in the number of selected events by comparing different Monte Carlo generators, as described in Section 4, was also taken as a systematic uncertainty.

7 Final states with four jets and at least two charged leptons

This section describes the event selection for final states resulting from the indirect decay of selectrons, smuons and staus via the coupling λ'. The final states consist of two charged leptons of the same flavour as the sleptons plus the decay products of the two neutralinos. These will be two jets plus a neutral or charged lepton for each neutralino. The identification of leptons and the preselection are the same as described in Section 6. The selection cuts were as follows:

(1) Lower and upper cuts in the ranges 0.5–0.7 and 0.75–1.2, respectively, were applied to the visible energy scaled by the centre-of-mass energy $E_{\text{vis}}/\sqrt{s}$, depending on the expected number of neutrinos. In addition, if some missing momentum was expected, a cut was made on the angle of the missing momentum with respect to the beam direction at $|\cos\theta| < 0.95$.

(2) The jets in the event were reconstructed using the Durham algorithm. The jet resolution parameter y_{45} at which the number of jets changes from four to five was required to be greater than 0.002. The $\log(y_{45})$ distribution is shown in Figure 3. It demonstrates the good discriminating power of this quantity. The visible disagreement in the peak position between data and Standard Model expectation was taken into account as a systematic uncertainty. This cut takes into account the high multiplicity of the signal events.

(3) At least two leptons of the flavour of the slepton had to be identified. To retain sensitivity to small mass differences between the slepton and the neutralino, the required scaled energy greater than 0.022 for the two electrons in the selectron case, the required momentum had to be greater than 4 GeV for both muons in the smuon case and the required momentum had to be greater than 3 GeV for both taus in the tau case, respectively.

(4) In addition to the leptons required in the previous cut (3), the leptons from the neutralino decay had to be identified. If two additional charged leptons with a different flavour to the slepton were expected, both had to be identified except in the case of two taus, where only one had to be identified. If a total of four leptons of the same flavour was expected, including those in cut (3), only three of them had to be identified. If only one additional lepton was expected, it had to be identified.

The scaled energy or momentum of the most energetic lepton had to be above a cut value varying between 0.044 and 0.08, depending on the topology. If a total of four leptons was required, for the second most energetic lepton a scaled energy or momentum larger than a cut value varying between 0.016 and 0.022, depending on the topology, was required.

(5) To make use of the isolation of the leptons in the signal, one or two of the identified leptons, depending on the expected topology, must be isolated. The isolation criterion was that there be no charged track within a cone of half opening angle φ, such that $|\cos\varphi| = 0.99$, around the track of the lepton.

Table 9 shows the efficiencies, the number of candidate events observed in the data and the number of background events for the selection at centre-of-mass energies from 189 GeV to 209 GeV, corresponding to an integrated luminosity of 599.6 pb^{-1}. Good agreement was found between the numbers of events expected and observed. The largest difference is observed for the final state with two taus and two neutrinos, where there is a 1.8 σ_{stat} excess in the number of data events. The main contribution to the Standard Model background comes from four-fermion processes; two-fermion multi-hadron events contribute up to 30% and other processes were negligible.

Systematic uncertainties

The systematic uncertainties on the signal efficiencies and on the expected number of background events were estimated in the same manner as in Section 6:

1. The statistical uncertainty from the limited size of the Monte Carlo samples.

2. The systematic uncertainty on the integrated luminosity (0.3 - 0.4%).
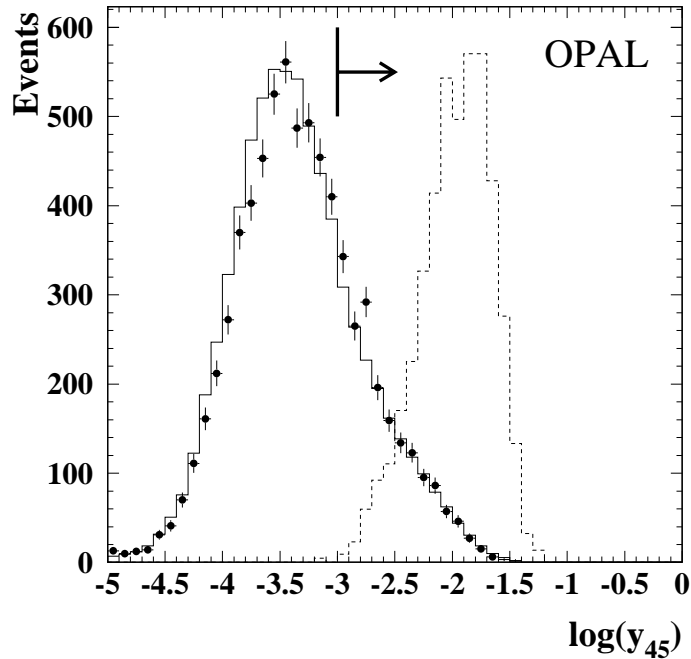
Figure 3: *Final states with four jets and at least two charged leptons: distribution of the variable*
y_{45} *before the cut on this variable for the indirect decay of selectrons into final states with four
jets and four electrons. The signal is shown as the dashed line for a selectron mass of 102 GeV
and a mass difference $\Delta m = m/2$. Data are shown as points and the sum of all Monte Carlo
background processes is shown as a solid line. Data used for this plot were collected in the
year 2000 at a luminosity weighted average centre-of-mass energy of 206.6 GeV. The visible
disagreement in the peak position between data and Standard Model expectation is taken into
account as a systematic uncertainty. The simulated signal events have arbitrary normalisation.
The arrow points into the region accepted by the cut. Uncertainties are statistical only.*

Physics process	Eff. (%)	Data	Tot. bkg MC	Data > 206 GeV	MC > 206 GeV
$\tilde{e}^+\tilde{e}^- \rightarrow$					
4 jets + 2e + 2e	39 − 69	13	$13.3 \pm 0.6 \pm 1.2$	2	$2.5 \pm 0.3 \pm 0.3$
4 jets + 2e + 2μ	25 − 53	2	$2.6 \pm 0.3 \pm 0.4$	0	$0.7 \pm 0.1 \pm 0.1$
4 jets + 2e + 2τ	6 − 25	14	$12.7 \pm 0.6 \pm 1.6$	5	$2.7 \pm 0.3 \pm 0.2$
4 jets + 2e + eν	17 − 40	16	$17.6 \pm 0.7 \pm 1.5$	2	$3.3 \pm 0.3 \pm 0.3$
4 jets + 2e + μν	21 − 52	16	$12.3 \pm 0.6 \pm 1.4$	4	$2.8 \pm 0.3 \pm 0.4$
4 jets + 2e + τν	2 − 12	7	$7.3 \pm 0.5 \pm 0.9$	1	$1.5 \pm 0.2 \pm 0.2$
4 jets + 2e + 2ν	6 − 17	6	$5.8 \pm 0.4 \pm 0.4$	2	$1.4 \pm 0.3 \pm 0.1$
$\tilde{\mu}^+\tilde{\mu}^- \rightarrow$					
4 jets + 2μ + 2e	34 − 54	2	$1.6 \pm 0.2 \pm 0.2$	0	$0.2 \pm 0.1 \pm 0.0$
4 jets + 2μ + 2μ	52 − 79	4	$2.9 \pm 0.3 \pm 0.6$	2	$0.7 \pm 0.1 \pm 0.2$
4 jets + 2μ + 2τ	9 − 32	2	$3.6 \pm 0.3 \pm 0.5$	0	$0.7 \pm 0.1 \pm 0.1$
4 jets + 2μ + eν	25 − 52	5	$4.4 \pm 0.3 \pm 0.8$	0	$1.0 \pm 0.2 \pm 0.3$
4 jets + 2μ + μν	30 − 51	4	$3.6 \pm 0.3 \pm 0.6$	2	$0.9 \pm 0.2 \pm 0.2$
4 jets + 2μ + τν	6 − 22	2	$2.3 \pm 0.2 \pm 0.3$	0	$0.4 \pm 0.1 \pm 0.0$
4 jets + 2μ + 2ν	15 − 35	6	$3.8 \pm 0.3 \pm 0.4$	0	$0.8 \pm 0.1 \pm 0.0$
$\tilde{\tau}^+\tilde{\tau}^- \rightarrow$					
4 jets + 2τ + 2e	19 − 52	9	$9.4 \pm 0.5 \pm 0.6$	1	$1.9 \pm 0.3 \pm 0.1$
4 jets + 2τ + 2μ	19 − 56	7	$8.8 \pm 0.4 \pm 1.4$	0	$2.2 \pm 0.2 \pm 0.5$
4 jets + 2τ + 2τ	7 − 22	53	$46.0 \pm 1.1 \pm 3.9$	6	$9.3 \pm 0.6 \pm 0.6$
4 jets + 2τ + eν	4 − 16	15	$12.1 \pm 0.6 \pm 1.1$	1	$2.1 \pm 0.3 \pm 0.2$
4 jets + 2τ + μν	4 − 14	12	$12.8 \pm 0.5 \pm 1.4$	1	$2.8 \pm 0.3 \pm 0.4$
4 jets + 2τ + τν	8 − 21	26	$24.9 \pm 0.8 \pm 2.3$	6	$5.1 \pm 0.4 \pm 0.5$
4 jets + 2τ + 2ν	3 − 8	83	$66.3 \pm 1.2 \pm 1.9$	16	$13.6 \pm 0.6 \pm 0.2$

Table 9: *Final states with four jets and at least two charged leptons for $\sqrt{s}$ = 189 - 209 GeV and for $\sqrt{s}$ > 206 GeV. Signal selection efficiencies, observed number of events in the data and background estimates from Standard Model processes. The first uncertainty on the background estimate is statistical and the second is systematic. The efficiencies are given for slepton masses larger than 45 GeV and for a signal at $\sqrt{s}$ = 207 GeV.*

3. The uncertainty due to the interpolation of efficiencies for mass values between the generated mass points (4%).

4. For the lepton identification, the highest uncertainty (4% for electrons) was taken for all flavours.

5. The systematic uncertainty arising from the modelling of the variables used in the selection. This results in a total systematic uncertainty on the efficiency of 5.2 - 13.4% for the selectron selection, of 5.2 - 12.0% for the smuon selection and of 5.2 - 19.3% for the stau selection.

6. From the studies of the fragmentation in Section 6, the systematic uncertainty for this analysis was estimated to be less than 1%.

The systematic uncertainty due to the uncertainty in the trigger efficiency was negligible, because of the requirement of at least eight good tracks.

The systematic uncertainty on the expected number of background events was again estimated to be less than 20% for all cases.

8 Final states with four jets and missing energy

Indirect decays of sneutrinos via a λ' coupling can lead to final states with four jets and a large amount of missing energy due to the four undetected neutrinos. The dominant background contribution comes from four-fermion processes, mainly $W^+W^- \rightarrow q\overline{q}\ell\nu$, and radiative or mismeasured two-fermion events. The selection procedure closely follows the one described in [16] with small changes required at the higher centre-of-mass energies. The selection procedure is described below:

(1) The event had to be classified as a multi-hadron final-state as described in [57].

(2) The visible energy of the event was required to be less than $0.75 \times \sqrt{s}$ to account for the undetectable neutrinos in the final state.

(3) To reject two-photon and radiative two-fermion events, the transverse momentum of the event should be larger than $0.075 \times \sqrt{s}$, the total energy measured in the forward calorimeter, gamma-catcher and silicon tungsten calorimeter should be less than 15 GeV, and there should be no significant energy deposit in the scintillating tile counters. The missing momentum should not point along the beam direction ($|\cos\theta_{\mathrm{miss}}| < 0.96$).

(4) The events were forced into four jets using the Durham jet-finding algorithm, and rejected if the jet resolution parameter y_{34} was less than 0.0008. All jets must contain at least one charged particle track.

(5) An additional cut was applied against semi-leptonic four-fermion events, vetoing events containing isolated leptons. The lepton veto is based on a NN routine [53], which was designed to identify tau leptons. The algorithm to select 1-prong tau candidates looks for high momentum isolated tracks, and therefore it is also suitable for vetoing leptons of other flavours. If any lepton candidate was found with a NN output larger than 0.97, the event was rejected.

26

Finally, a likelihood selection was employed to classify the remaining events as two-fermion, four-fermion or signal-like processes. The method is described in [58]. The signal reference histograms were produced separately for first generation sneutrinos where t-channel production is also expected and for second or third generation sneutrinos with s-channel production only. For a given centre-of-mass energy, all the generated signal events with the coupling λ'_{121}, whatever their masses, were used with equal weight to form the reference distributions. The information from the following variables was combined:

- the effective centre-of-mass energy [59] of the event;
- the transverse momentum of the event;
- the cosine of the polar angle of the missing momentum vector;
- the D event-shape parameter [60] which provides information about the planar nature of an event;
- the aplanarity of the event which measures the transverse momentum component out of the event plane and which is defined as $3/2$ times the smallest eigenvalue of the sphericity tensor;
- the logarithm of y_{34};
- the highest track momentum;
- the highest electromagnetic cluster energy;
- the number of lepton candidates in the event with a NN output larger than 0.5;
- the mass of the hadronically decaying W after a kinematic fit to the $W^+W^- \to q\bar{q}\ell\nu$ hypothesis;
- the cosine of the smallest jet opening angle, defined by the half-angle of the smallest cone containing 68% of the jet energy;

The distribution of the likelihood output is shown in Figure 4 for the data, the estimated background and a simulated signal sample in the electron sneutrino selection. The event was rejected if its likelihood output was smaller than 0.95.

Table 10 shows the results of the different selections on the data collected at centre-of-mass energies between 189 GeV and 209 GeV corresponding to an integrated luminosity of $610.6 \ \mathrm{pb}^{-1}$. The efficiencies shown in Table 10 are quoted for the coupling λ'_{121} and $\Delta m \leq m_{\tilde{\nu}}/2$. For $\Delta m > m_{\tilde{\nu}}/2$, the detection efficiency drops by a factor 2 to 4, depending on $m_{\tilde{\nu}}$ and Δm, due to the larger fraction of missing energy and lower energy final state jets. For a mass difference of 5 GeV, the primary neutrinos carry away less energy and the efficiency increases by an absolute value of about 10%. The efficiency is small for light sneutrino masses due to the effect of the initial-state radiation and the larger boost of the particles, which make the event similar to the QCD two-fermion background. About 94% of the events expected from the Standard Model originate from four-fermion processes.

Physics process	Eff. (%)	Data	Tot. bkg MC	Data > 206 GeV	MC > 206 GeV
$\tilde{\nu}_e \overline{\tilde{\nu}}_e \to 4\ jets + E_{miss}$	1 − 25	54	$39.5 \pm 0.5 \pm 4.3$	8	$8.2 \pm 0.2 \pm 1.3$
$\tilde{\nu}_\mu \overline{\tilde{\nu}}_\mu, \tilde{\nu}_\tau \overline{\tilde{\nu}}_\tau \to 4\ jets + E_{miss}$	1 − 22	57	$39.4 \pm 0.5 \pm 4.3$	9	$8.3 \pm 0.2 \pm 2.0$

Table 10: *Final states with four jets and missing energy for $\sqrt{s} = 189$ - 209 GeV and for $\sqrt{s} > 206$ GeV: signal selection efficiencies for sparticle masses above 45 GeV and $\Delta m \leq m_{\tilde{\nu}}/2$, observed numbers of events in the data and background estimates from Standard Model processes. The first uncertainty on the background estimate is statistical and the second is systematic. The numbers of observed events are highly correlated between the selections.*
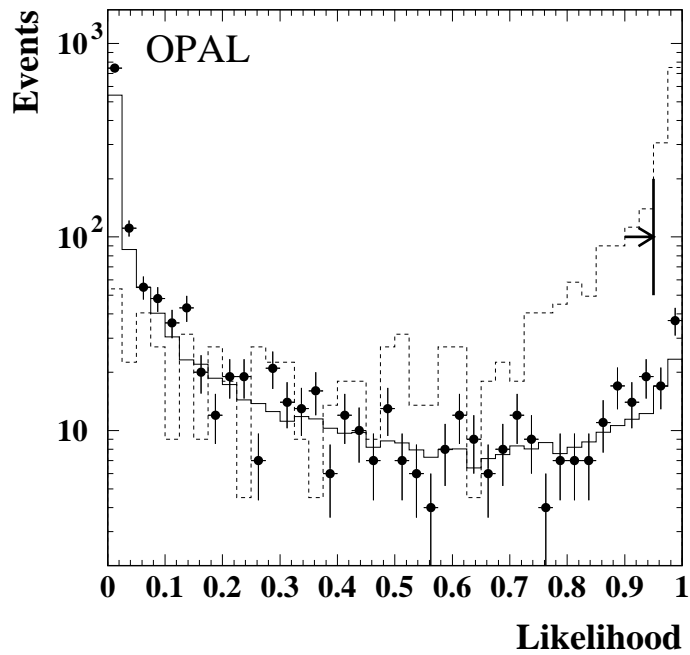
Figure 4: *Final states with four jets and missing energy, electron sneutrino selection at $\sqrt{s} = 189\text{-}209$ GeV: distribution of the likelihood output for the selected events in the data (points with error bars), the estimated background normalised to the integrated luminosity of the data (solid line) and a simulated sample of electron sneutrino pair-production for $m_{\tilde{\nu}_e} = 102.5$ GeV with arbitrary normalisation (dashed line). Uncertainties are statistical only. The arrow indicates the cut position.*

The observed approximately 2 σ_{stat} excess in the data spreads over the different centre-of-mass energies and it is concentrated in the $0.075 < p_{\mathrm{T}}/\sqrt{s} < 0.15$ region, not favoured by events with pair-produced high mass sleptons. An excess appears from the first steps of the selection. After cut (5), 1445 events were observed for 1240 expected from Standard Model processes. As seen in Figure 4, there is a significant excess in the low likelihood region, which is expected to be almost equally populated by two- and four-fermion events.

Systematic uncertainties

The following sources of uncertainties were considered on the selection efficiencies (all quoted uncertainties are relative):

1. The limited MC statistics (5.4−28.7%).

2. The statistical and systematic uncertainties on the luminosity measurement (0.3−0.4%).

3. The modelling of the preselection variables (2.2−2.5%).

4. The modelling of the variables used in the likelihood selection (20.9−23.4%).

5. The modelling of the lepton veto (1%).

6. The interpolation of efficiencies (2.7−5.2%).

Similarly the background estimate is affected by uncertainties due to:

1. The limited MC statistics (1.2%).

2. The statistical and systematic uncertainties on the luminosity measurement (0.3−0.4%).

3. The modelling of the preselection variables (8.6−9.6%).

4. The modelling of the variables used in the likelihood selection (27.8−29.1%).

5. The modelling of the lepton veto (1%).

6. The imperfect knowledge of Standard Model cross-sections (2%).

7. The imperfect simulation of four-fermion processes determined by comparing the predictions of grc4f, KORALW and KandY (16%).

The total systematic uncertainty excluding MC statistics ranges from 21.2 to 24.3% on the signal detection efficiency and from 33.3 to 34.6% on the background rate.

The effect of the modelling of the preselection and likelihood variables was estimated for each variable using the transformation described in Section 6. Applying the same analysis with unchanged reference histograms to calculate the likelihood, the difference in the MC expectation due to the transformation was considered as the systematic uncertainty. The largest contributions both for the signal and for the background come from the modelling of

the logarithm of y_{34}, the energy of the most energetic electromagnetic cluster and the cosine of the smallest jet opening angle in the likelihood selection.

The uncertainty introduced by interpolating the signal efficiencies between simulated signal masses was estimated in the following way: the signal efficiencies were randomly smeared within their statistical uncertainty and the resulting numbers were used in the interpolation. This process was repeated 100 times, and the absolute differences between the original and the smeared fits were averaged. For each slepton mass, the mean difference was taken as a measure of the systematic uncertainty. There is no interpolation between the generated centre-of-mass energies: the efficiency determined from the signal sample with closest generated centre-of-mass energy was always taken. The largest difference between the actual and the generated centre-of-mass energies is about 3 GeV, and its effect on the result is negligible.

The inefficiency due to the forward energy veto, by which both the signal efficiencies and the background estimates were decreased, was found to vary between 1.9 and 3.7% by studying randomly triggered events.

9 Final states with four jets and no missing energy

Direct decays of sleptons via λ' couplings and squarks via λ'' couplings can result in final states with four well-separated, high multiplicity hadron jets and a large amount of visible energy. The main background comes from four-fermion processes, dominantly $W^+W^- \rightarrow q\bar{q}q\bar{q}$, with some contribution from $q\bar{q}(\gamma)$ events with hard gluon emission.

The analysis is similar to the one of [16]. It consists of a cut-based preselection to reduce the two-photon and two-fermion backgrounds and a likelihood selection to suppress the contribution from Standard Model four-fermion events. The preselection consists of the following steps:

(1) The event has to be classified as a multi-hadron final state as described in [57].

(2) The effective centre-of-mass energy of the event, $\sqrt{s'}$ [59], was required to be greater than $0.82 \times \sqrt{s}$ to reject events with large initial state radiation.

(3) To ensure that the events were well contained in the active region of the detector, the visible energy should be larger than $0.7 \times \sqrt{s}$.

(4) The events were forced into four jets using the Durham jet-finding algorithm, and rejected if the jet resolution parameter y_{34} was less than 0.0025. Moreover, all jets must contain at least one charged particle.

(5) A four-constraint kinematic fit (4C-fit) requiring energy and momentum conservation for the jet four-momenta should yield a χ^2 probability larger than 10^{-5}.

(6) To test the compatibility with pair-produced equal mass objects and to obtain the best possible resolution for the reconstructed mass of a hypothetical sfermion, the jet four-momenta were refitted requiring energy and momentum conservation and equal jet pair invariant masses (5C-fit). The event was kept if at least one of the three jet pairing combinations has a χ^2 probability larger than 10^{-5}. The combination with the highest χ^2 probability was considered later in the mass reconstruction.

(7) A cut was applied on the C event shape parameter [60] which provides an effective measure of the multi-jet structure of the event, $C > 0.45$.

Finally, a likelihood selection was employed to classify the remaining events. Three event classes were used: signal, two-fermion and four-fermion. The signal reference histograms were produced separately for selectrons where t-channel production plays an important role, for electron-sneutrinos where the t-channel process also contributes but to a lesser extent and for second or third generation neutral and charged sleptons with s-channel production only. Since squarks are coloured particles they were treated separately. For a given centre-of-mass energy, all the generated masses were used with equal weight to form the reference distributions. The following variables were used as inputs to the likelihood calculation:

- the cosine of the polar angle of the thrust axis;
- the cosine of the smallest angle between the directions of any two of the four reconstructed jets;
- the difference between the largest and smallest jet energy after the 4C-fit;
- the smallest difference between the reconstructed masses of the two jet pairs from any of the three possible jet pair combinations;
- the cosine of the direction of the jet pair momentum multiplied by the charge of the jet pair[6] for the combination with the highest χ^2 probability given by the 5C-fit.

Events were accepted if their likelihood output was larger than 0.5 for selectrons, 0.55 for electron sneutrinos, 0.6 for second and third generation neutral and charged sleptons and 0.7 for squarks.

Table 11 shows the numbers of selected data and expected background events for the different selections at centre-of-mass energies from 189 GeV to 209 GeV, corresponding to an integrated luminosity of 610.6 pb^{-1}. More than 92% of the events expected from the Standard Model originate from four-fermion processes. Figure 5 shows, as an example, the jet pair invariant mass distribution of the selected events after the 5C-fit in the selectron selection: the dominance of W$^+$W$^-$ production in the Standard Model background is clearly visible from the strongly peaked distribution around the W boson mass. The jet pair invariant mass resolution for signal events is $\sigma \approx 0.6-1.6$ GeV, depending on the type and the mass of the produced sparticle. To profit from the good mass resolution, events were selected if they were in a $\pm 2\sigma$ mass window around the test mass. The efficiencies in Table 11 are given after the mass selection and all correspond to the Yukawa coupling giving the worst result.

Systematic uncertainties

The systematic uncertainties were estimated in the same manner as in the search for four jets and missing energy. For the selection efficiency the following sources of uncertainties were considered:

1. The limited MC statistics (3.1−11.9%).

2. The statistical and systematic uncertainties on the luminosity measurement (0.3−0.4%).

---

[6]The charge of the jet pair was calculated as $\Sigma q_{(i)} p_{\mathrm{L}(i)}^{0.5}$, where the sum goes over each track within the two jets, $q_{(i)}$ is the charge of the track and $p_{\mathrm{L}(i)}$ is its momentum parallel to the jet direction. A charge of $+1$ was assigned to the jet pair with the larger charge, and a charge of -1 to the other.

Physics process	Eff. (%)	Data	Tot. bkg MC	Data > 206 GeV	MC > 206 GeV
$\tilde{e}^+\tilde{e}^- \to 4\ jets$	$14 - 46$	922	$917 \pm 10 \pm 69$	193	$210 \pm 5 \pm 38$
$\tilde{\nu}_e\overline{\tilde{\nu}}_e \to 4\ jets$	$15 - 43$	760	$762 \pm 8 \pm 56$	158	$175 \pm 4 \pm 30$
$\tilde{\mu}^+\tilde{\mu}^-, \tilde{\tau}^+\tilde{\tau}^-,$ $\tilde{\nu}_\mu\overline{\tilde{\nu}}_\mu, \tilde{\nu}_\tau\overline{\tilde{\nu}}_\tau \to 4\ jets$	$9 - 39$	584	$589 \pm 6 \pm 43$	123	$138 \pm 3 \pm 24$
$\tilde{q}\overline{\tilde{q}} \to 4\ jets$	$9 - 37$	393	$393 \pm 5 \pm 29$	81	$89 \pm 2 \pm 15$

Table 11: *Final states with four-jets and no missing energy for $\sqrt{s}$ = 189 - 209 GeV and for $\sqrt{s}$ > 206 GeV: signal selection efficiencies for sparticle masses above 45 GeV, observed numbers of events in the data and background estimates from Standard Model processes. The first uncertainty on the background estimate is statistical and the second is systematic. The efficiencies are given after the mass selection described in the text while the data and the background correspond to the whole mass region. The inefficiency related to the fragmentation model was taken into account for the squark result. There is a significant correlation amongst the different selections at the same centre-of-mass energy.*
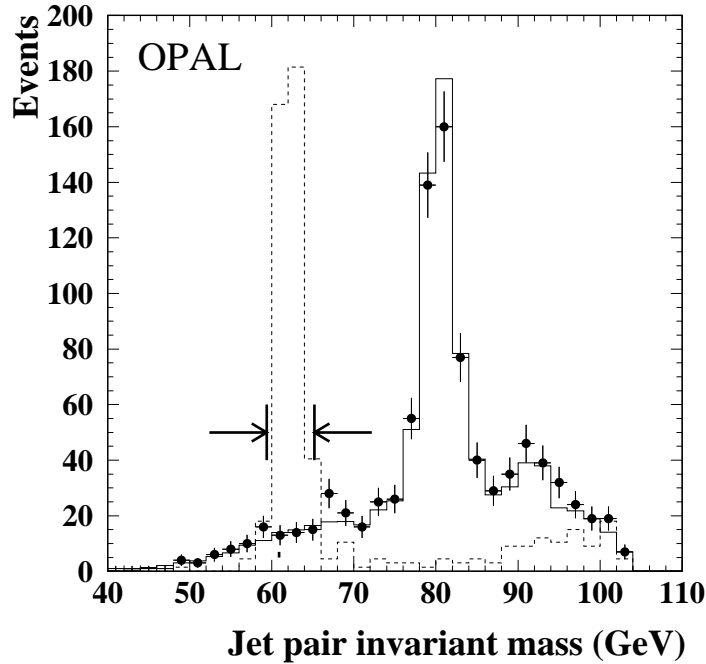
Figure 5: *Final states with four jets and no missing energy, selectron selection at $\sqrt{s}$ = 189-209 GeV: distribution of the reconstructed mass for the selected events in the data (points with error bars), the estimated background normalised to the integrated luminosity of the data (solid line) and a simulated sample of selectron pair-production for $m_{\tilde{e}}$ = 62 GeV with arbitrary normalisation (dashed line). Uncertainties are statistical only. The arrows indicate the mass window which would be selected for the specific case of the signal shown.*

3. The modelling of the preselection variables (15.9−18.2%, largest contribution of 10.2−15.3% from the χ^2 probability of the 4C-fit).

4. The modelling of the variables used in the likelihood selection (6.6−10.9%).

5. The interpolation of efficiencies (1.6−3.2%).

The background estimate is subject to uncertainties due to

1. The limited MC statistics (1.1%).

2. The statistical and systematic uncertainties on the luminosity measurement (0.3−0.4%).

3. The modelling of the preselection variables (13.2−16.3%, largest contribution of 8.7−13.3% from the χ^2 probability of the 4C-fit).

4. The modelling of the variables used in the likelihood selection (4.5−10.7%).

5. The imperfect knowledge of Standard Model cross-sections (2%).

6. The imperfect simulation of four-fermion processes (3.3−6.4%).

The total systematic uncertainty excluding MC statistics ranges from 17.3 to 21.5% on the signal detection efficiency and from 16.4 to 18.3% on the background rate.

As explained in Section 4, the squark pair Monte Carlo samples were produced using an independent fragmentation model which gives narrower, better separated jets and therefore optimistic selection efficiencies. To estimate this effect, the efficiencies were compared for smuon Monte Carlo samples with independent and string fragmentation models. From this study an additional relative inefficiency of 7.9% to 36.9% was derived, by which the squark detection efficiencies were decreased. For the same reason, the squark results at 183 GeV [16] were updated using a similar procedure and these new results are used later in the combination.

10   Interpretation

No significant excess of signal-like events was observed in the data with respect to the expected background for any analysis listed in Table 1. Production cross-section and mass limits were therefore computed using the data collected at LEP from centre-of-mass energies ($\sqrt{s}$) between 189 GeV and 209 GeV and then combined with results obtained using data at lower energies [16]. These limits take into account indirect limits obtained from the study of the Z^0 width at LEP1 and therefore concern only sparticle masses above 45 GeV. All limits presented here are quoted at the 95% confidence level.

Two approaches were used to present sfermion production limits. In the first, upper limits on the production cross-sections were calculated as functions of the sfermion masses with minimal model assumptions. These upper limits in general do not depend on the details of the SUSY models, except for the assumptions that the sparticles are pair-produced and that only one λ-like coupling at a time is non-zero [16]. In the second approach, limits on the sfermion masses were calculated in an R-parity violating framework analogous to the CMSSM, where

mass limits were derived for $\tan\beta = 1.5$ and $\mu = -200$ GeV. This choice of parameters, which generally results in small sfermion production cross-sections, is a convenient benchmark for limit setting and is used by other collaborations, so results may be compared and combined. For the indirect sfermion decays, we used the branching ratios for the decay $\tilde{f} \rightarrow f\tilde{\chi}_1^0$ predicted by the CMSSM, and we conservatively assumed no experimental sensitivity to any other decay mode. The branching ratio for direct decay was always assumed to be unity, as only one λ coupling at a time was allowed to be different from zero.

As in [16], the relative branching ratios of the neutralino into a final state with a charged or a neutral lepton were varied between 0 and 1 to avoid a dependence of the results on the CMSSM parameters. A likelihood ratio method [61] was used to determine an upper limit for the cross-section. This results in a cross-section limit as a function of the branching ratio and the sfermion mass. A limit independent of the branching ratio was determined by taking the lowest limit at each sfermion mass. For the direct decays, the final states are fully determined by the indices of the coupling considered.

In the following sections, cross-section limits are shown for the various direct and indirect decays studied in this paper and are listed in Table 1. In each cross-section plot for the decays via λ couplings, the curves corresponding to the highest and the lowest cross-section limits are shown. Generally, the highest excluded cross-section comes from final states with a maximum number of muons and no taus, while the worst results come from final states with many taus, due to their lower detection efficiency. In the other cases, only the curve corresponding to the worst cross-section limit is shown amongst all possible cross-section limits resulting from the couplings considered.

In the CMSSM framework, the exclusion regions for the indirect decays are valid for $m_{\tilde{\chi}_1^0} \geq 10$ GeV, to ensure prompt decays. The region in the plane ($m_{\tilde{\ell}}$, $m_{\tilde{\chi}_1^0}$) corresponding to $m_{\tilde{\chi}_1^0} < 10$ GeV, where the lifetime of sparticles would be sufficiently long to produce a secondary decay vertex, clearly detached from the primary vertex, or even outside the detector, is labelled "Lifetime signature" and is not excluded by these searches.

For indirect sparticle decays, mass lower limits are quoted for $\tilde{\chi}_1^0 = 10$ GeV, referred to as a low-mass $\tilde{\chi}_1^0$. In the small Δm region ($\Delta m = m_{\tilde{\ell}} - m_{\tilde{\chi}_1^0} < 5$ GeV), the final state charged leptons resulting from the charged slepton decay into a charged lepton and a neutralino may not be detected due to the small phase space available. This region is excluded for the charged sleptons decaying indirectly via a λ coupling. For the charged sleptons decaying indirectly via a λ' coupling, no exclusion was possible in this region. The exclusion region for the direct decays is independent of Δm.

The production cross-section for left-handed charged sleptons is always larger than that for right-handed charged sleptons; therefore, whenever applicable for the superpotential form given in Equation (1), results are conservatively quoted for right-handed charged sleptons.

10.1 Selectron limits

Upper limits on the cross-sections of pair-produced selectrons followed by the direct decay via a λ coupling are shown in Figure 6. Due to the structure of the $LL\overline{E}$ term and the presence of a neutrino in the decay products, only left-handed sleptons can decay via this term, the other decays being suppressed. Since the selection efficiency for this analysis only depends on the

final states and not on the parent slepton type, this limit also holds for the pair production of smuons and staus decaying directly via a λ coupling.
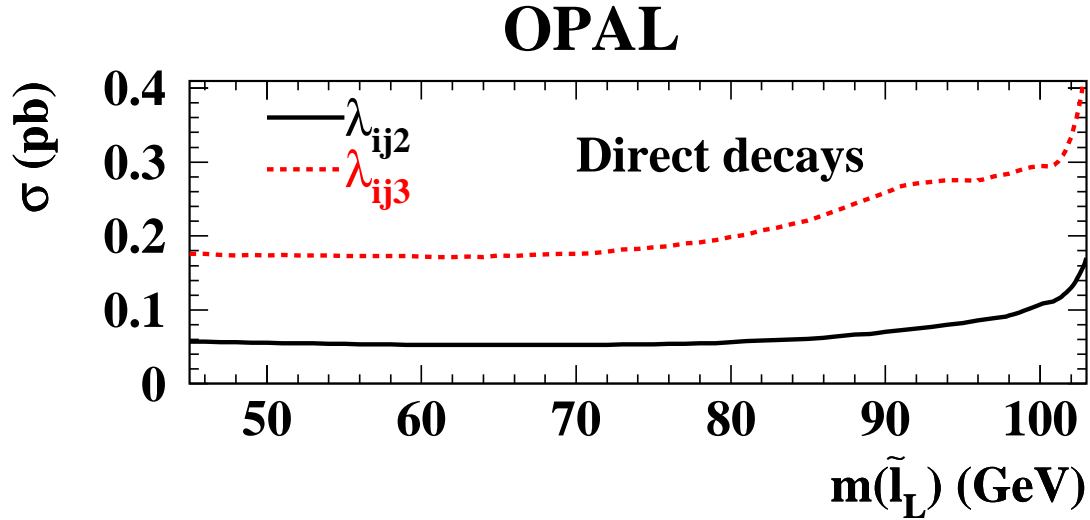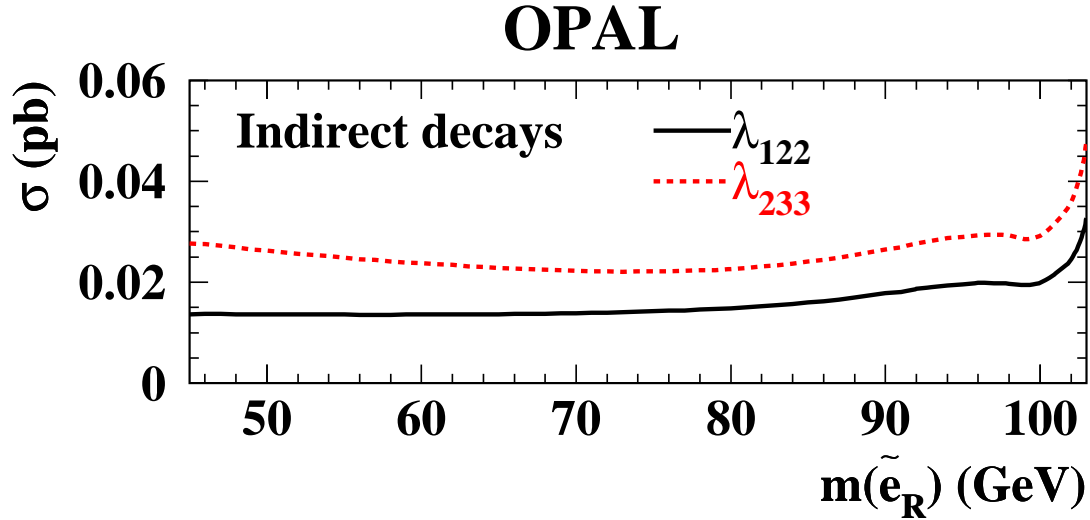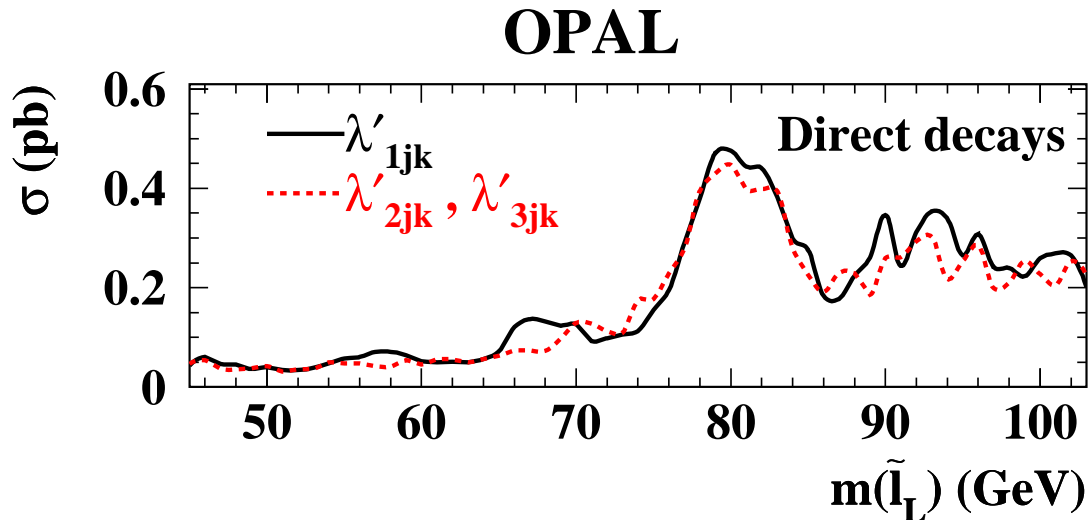

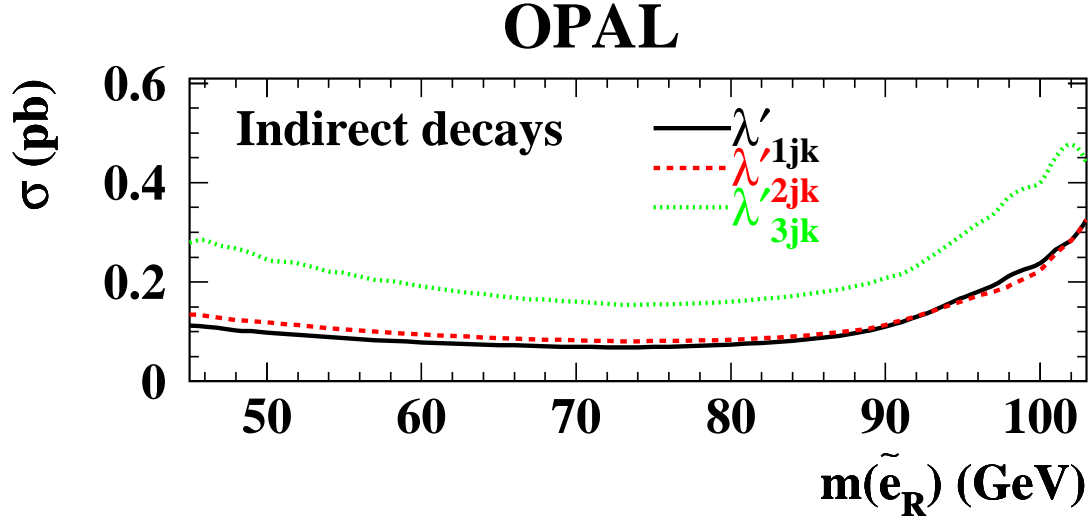Figure 6: *Charged slepton direct decays via a λ coupling: upper limits at the 95% C.L. on the pair-production cross-sections of left-handed sleptons decaying directly. The dashed line shows the lowest upper limit ($\tau\nu\tau\nu$ final states) while the solid line shows the highest one ($\mu\nu\mu\nu$ final states).*

Upper limits on the cross-sections of pair-produced selectrons decaying indirectly via a λ coupling are shown in Figure 7.

Upper limits on the cross-sections of pair-produced selectrons decaying directly via a $\lambda^{'}$ coupling to a four-jet final state are shown in Figure 8. The peak structure visible in the figure at approximately the mass of the W-boson comes from irreducible background due to W pair-production.

Upper limits on the cross-sections of pair-produced selectrons decaying indirectly via a $\lambda^{'}$ coupling are shown in Figure 9 for the indirect decay of a $\tilde{e}_R$ in the electron channel, in the muon channel and in the tau channel.

In the CMSSM, the selectron pair-production cross-section is enhanced by the presence of a t-channel diagram. The exclusion limits for selectrons decaying via a λ coupling are shown in Figure 10(a). In the region where the neutralino is heavier than the selectron, only direct decays are possible. When the neutralino is lighter than the selectron, the indirect decays are expected to be dominant. The exclusion refers to right-handed selectrons for the indirect decays and to left-handed selectrons for direct decays.

The exclusion limits for selectrons decaying via a $\lambda^{'}$ coupling are shown in Figure 10(b). The lower mass limits for selectrons decaying directly or indirectly via a λ or a $\lambda^{'}$ coupling are included in Table 12. The mass limits for the indirect decays are quoted for a low-mass $\tilde{\chi}_1^0$ (10 GeV).

OPAL

Figure 7: *Selectron indirect decays via a λ coupling: upper limits at the 95% C.L. on the pair-production cross-sections of a right-handed $\tilde{e}_R$ decaying indirectly. The dashed line shows the lowest upper limit ($e\tau\tau\nu e\tau\tau\nu$ final state) while the solid line shows the highest one ($e\mu\mu\nu e\mu\mu\nu$ final state).*

OPAL

Figure 8: *Charged slepton direct decays via a λ′ coupling: upper limits at the 95% C.L. on the pair-production cross-sections of $\tilde{e}$ (solid line) and $\tilde{\mu}/\tilde{\tau}$ (dashed line) decaying directly.*
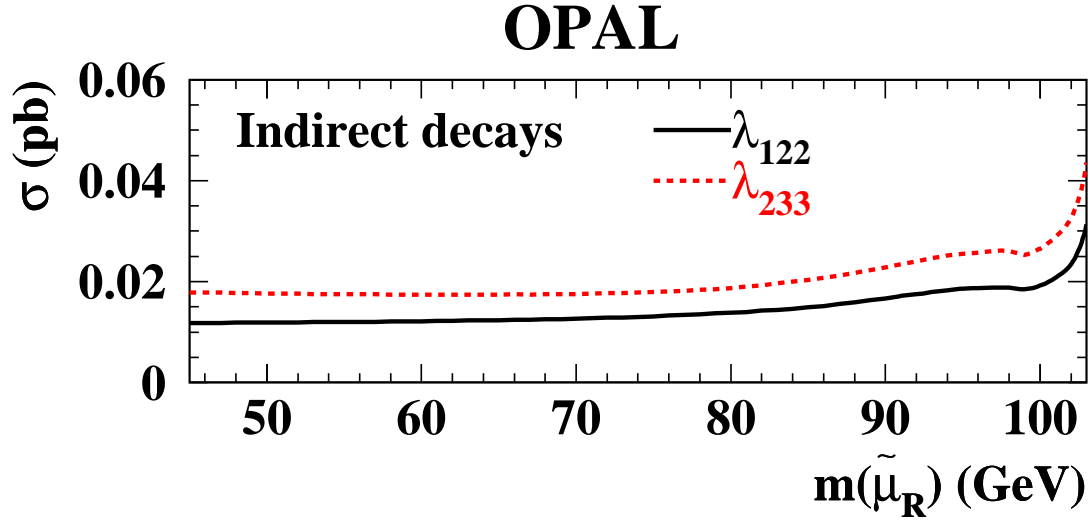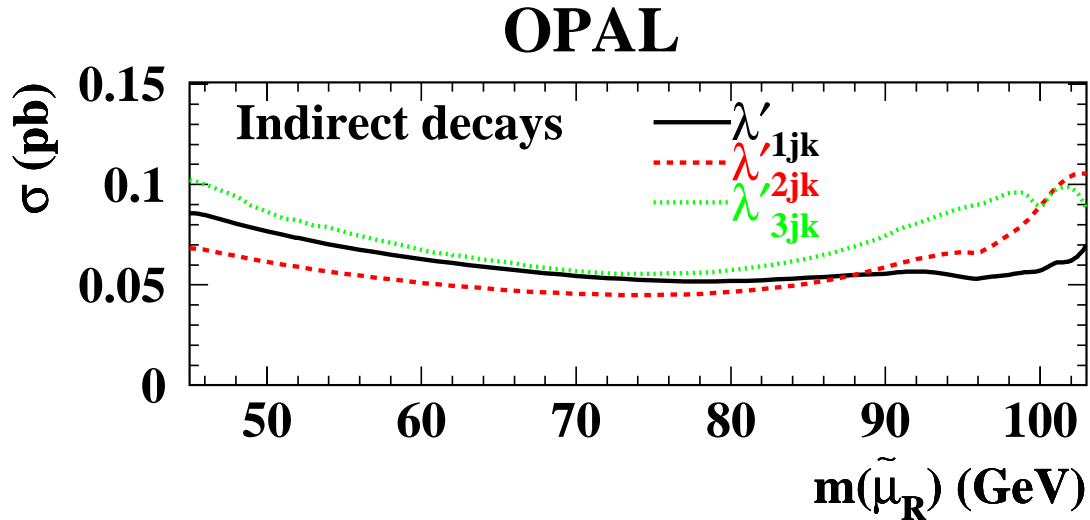
36

Figure 9: *Selectron indirect decays via a λ' coupling: upper limits at the 95% C.L. on the pair-production cross-sections the of a $\tilde{e}_R$ decaying indirectly in the electron channel (solid line), in the muon channel (dashed line) and in the tau channel (dotted line).*

Charged Slepton Lower Mass Limits(GeV)				
Species	λ		λ'	
	Direct	Indirect	Direct	Indirect
$\tilde{e}$	89	99	89	92
$\tilde{\mu}$	74	94	75	87
$\tilde{\tau}$	74	92	75	-

Table 12: *Lower mass limits for charged sleptons decaying directly or indirectly via a λ or a λ' coupling. The mass limits for indirect decays are quoted for a low-mass $\tilde{\chi}_1^0$ (10 GeV). The limits refer to right-handed charged sleptons for the indirect decays and to left-handed charged sleptons for direct decays.*
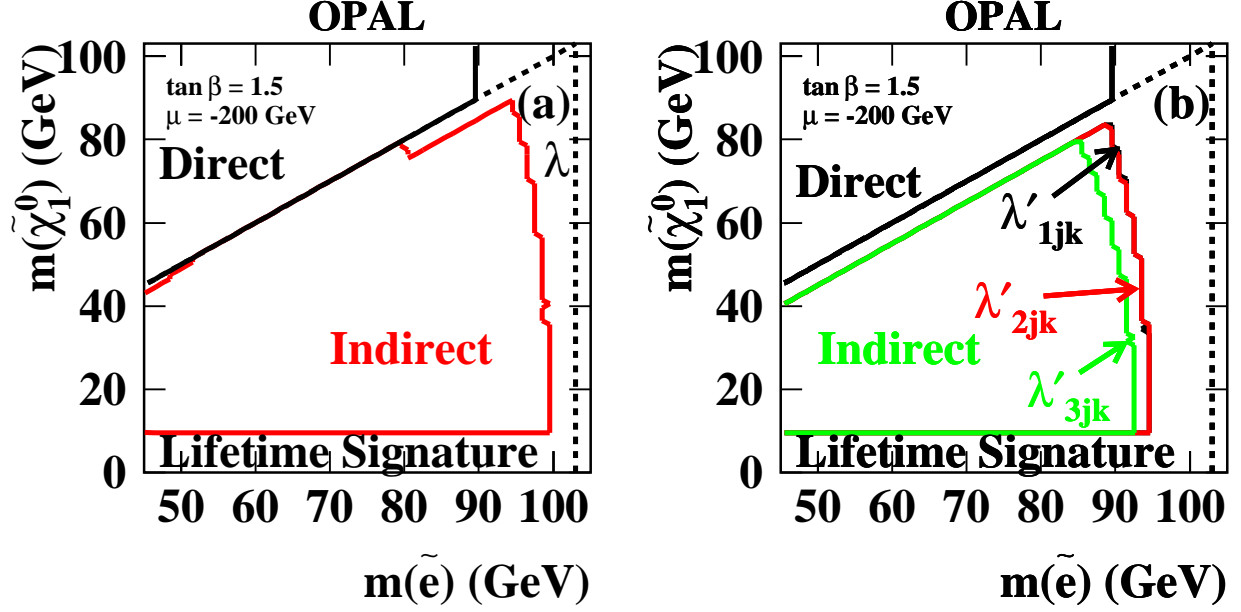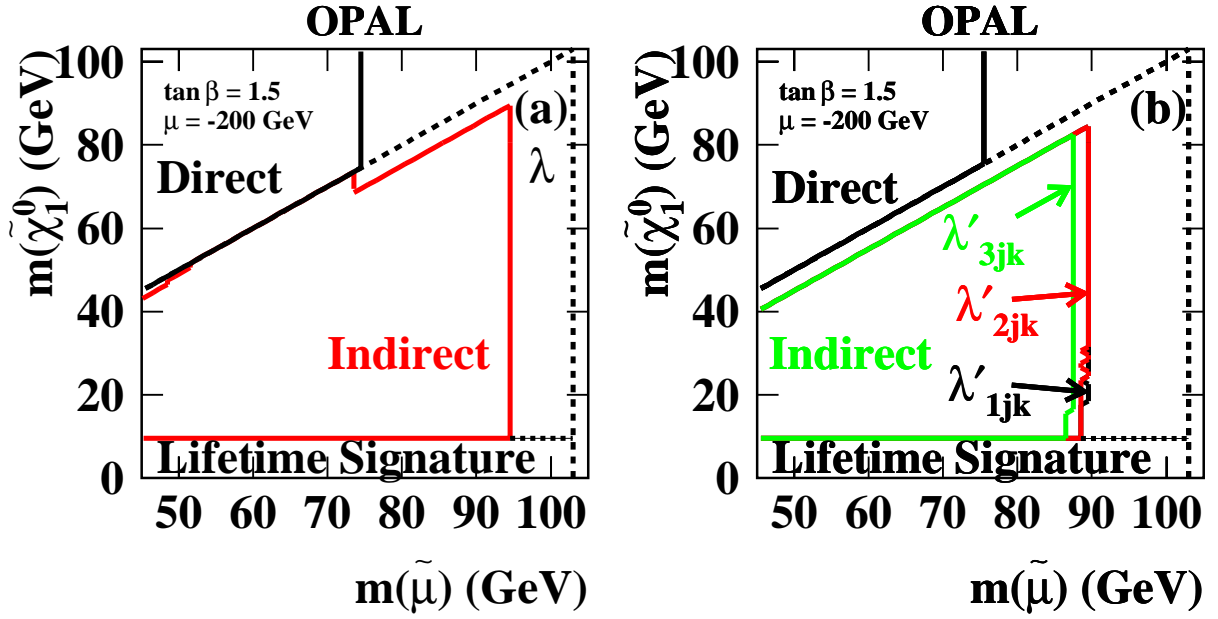
Figure 10: *CMSSM exclusion region for $\tilde{e}^+\tilde{e}^-$ production in the $(m_{\tilde{e}}, m_{\tilde{\chi}_1^0})$ plane at 95% C.L. for (a) a λ coupling and (b) a λ' coupling. The limits for λ' couplings are presented separately according to the first index. For the direct decays, the exclusion is shown for the only possible case of $\tilde{e}_L\tilde{e}_L$. The kinematic limit is shown by the dashed lines.*

10.2 Smuon limits

Upper limits on the cross-sections of pair-produced smuons decaying directly via a λ coupling are shown in Figure 6.

Figure 11 shows upper limits on the cross-sections of pair-produced smuons followed by an indirect decay via a λ coupling.

Upper limits on the cross-sections for pair-produced smuons decaying indirectly via a λ' coupling are shown in Figure 12.

Upper limits on the cross-sections of pair-produced smuons decaying directly via a λ' coupling to a four-jet final state are shown in Figure 8.

The exclusion limits for smuons decaying via a λ coupling are shown in Figure 13(a). The exclusion limits for smuons decaying via a λ' coupling are shown in Figure 13(b). The lower mass limits for smuons decaying directly or indirectly via a λ or a λ' coupling are included in Table 12.

10.3 Stau limits

Upper limits on the cross-sections of pair-produced staus decaying directly via a λ coupling are shown in Figure 6.

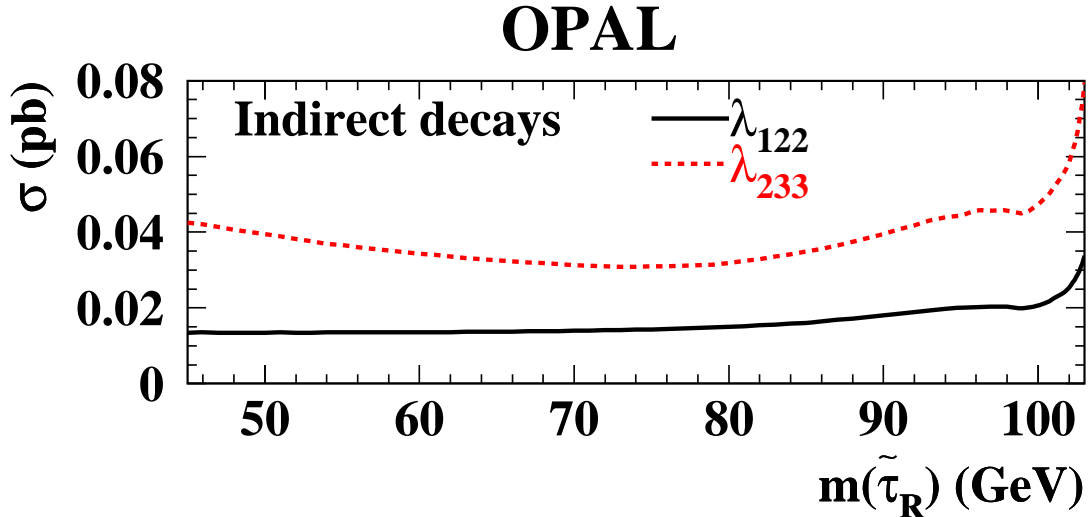Upper limits on the cross-sections of pair-produced staus decaying indirectly via a λ coupling are shown in Figure 14.

Figure 11: *Smuon indirect decays via a λ coupling: upper limits at the 95% C.L. on the pair-production cross-sections of right-handed $\tilde{\mu}_R$ decaying indirectly. The dashed line shows the lowest upper limit ($\mu\tau\tau\nu\mu\tau\tau\nu$ final state) while the solid line shows the highest one ($\mu\mu\mu\nu\mu\mu\mu\nu$ final state).*

Figure 12: *Smuon indirect decays via a λ' coupling: upper limits at the 95% C.L. on the pair-production cross-sections of $\tilde{\mu}_R$ decaying indirectly in the electron channel (solid line), in the muon channel (dashed line) and in the tau channel (dotted line).*

Figure 13: *CMSSM exclusion regions for $\tilde{\mu}^+\tilde{\mu}^-$ production in the $(m_{\tilde{\mu}}, m_{\tilde{\chi}_1^0})$ plane at 95% C.L. for (a) a λ coupling and (b) a λ' coupling. The limits for λ' couplings are presented separately according to the flavour of the lepton in the decay. For the direct decays, the exclusion region is shown for the case $\tilde{\mu}_L\tilde{\mu}_L$. The kinematic limit is shown by the dashed lines.*

Figure 14: *Stau indirect decays via a λ coupling: upper limits at the 95% C.L. on the pair-production cross-sections of right-handed $\tilde{\tau}_R$ decaying indirectly. The dashed line shows the lowest upper limit ($\tau\tau\nu\tau\tau\nu$ final state), while the solid line shows the highest one ($\tau\mu\mu\nu\tau\mu\mu\nu$ final state).*

Figure 15 shows upper limits on the cross-sections for pair-produced staus decaying indirectly via a λ' coupling in the electron channel. Since the neutralino can decay into final states with either a charged lepton or a neutrino, limits are set by varying this branching ratio for the neutrino final state between 0 and 1. For the stau decay in the electron, muon and tau channels, the lowest limits arise in all cases for the neutrino branching ratio of 1. This means that the limits for the muon and tau channels are identical to the electron channel limit shown.
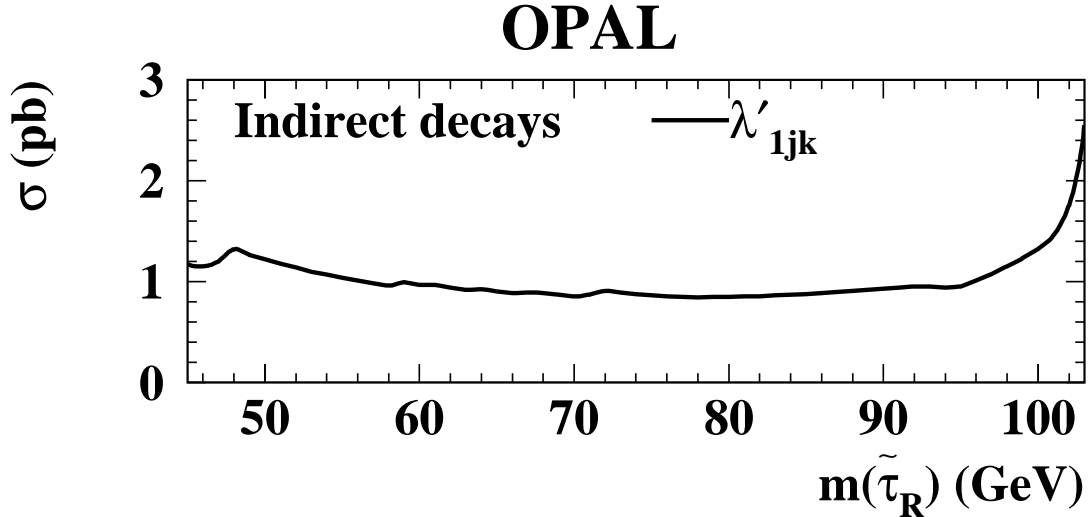
Figure 15: *Stau indirect decays via a λ' coupling: upper limit on the pair-production cross-sections for the indirect decay of a $\tilde{\tau}_R$ in the electron channel. The indirect decay of a $\tilde{\tau}_R$ in the muon channel and the indirect decay of a $\tilde{\tau}_R$ in the tau channel yield identical results.*

Upper limits on the cross-sections of pair-produced staus decaying directly via a λ' coupling to a four-jet final state are shown in Figure 8.

The exclusion limits in the $(m_{\tilde{\tau}}, m_{\tilde{\chi}_1^0})$ plane for staus decaying via a λ coupling are shown in Figure 16(a). The exclusion limits for staus decaying via a λ' coupling are shown in Figure 16(b). The lower mass limits for staus decaying directly or indirectly via a λ or a λ' coupling are included in Table 12. For indirect decays via a λ' coupling, no exclusion was possible since the theoretical cross-sections were smaller than the experimental limits in all cases.

10.4   Sneutrino limits

Upper limits on the cross-sections of pair-produced sneutrinos decaying directly via a λ coupling are shown in Figure 17.

Upper limits on the cross-sections of pair-produced sneutrinos decaying indirectly via a λ coupling are shown for $\Delta m \leq m_{\tilde{\nu}}/2$ in Figure 18. These limits degrade for $\Delta m > m_{\tilde{\nu}}/2$ due to the larger fraction of missing energy and lower energy final state charged leptons.

Upper limits on the cross-sections of pair-produced sneutrinos decaying directly via a λ' coupling to a four-jet final state are shown in Figure 19.

Upper limits on the cross-sections of pair-produced sneutrinos decaying indirectly via a λ' coupling to a four-jet final state with missing energy are shown for $\Delta m \leq m_{\tilde{\nu}}/2$ in Figure 20.
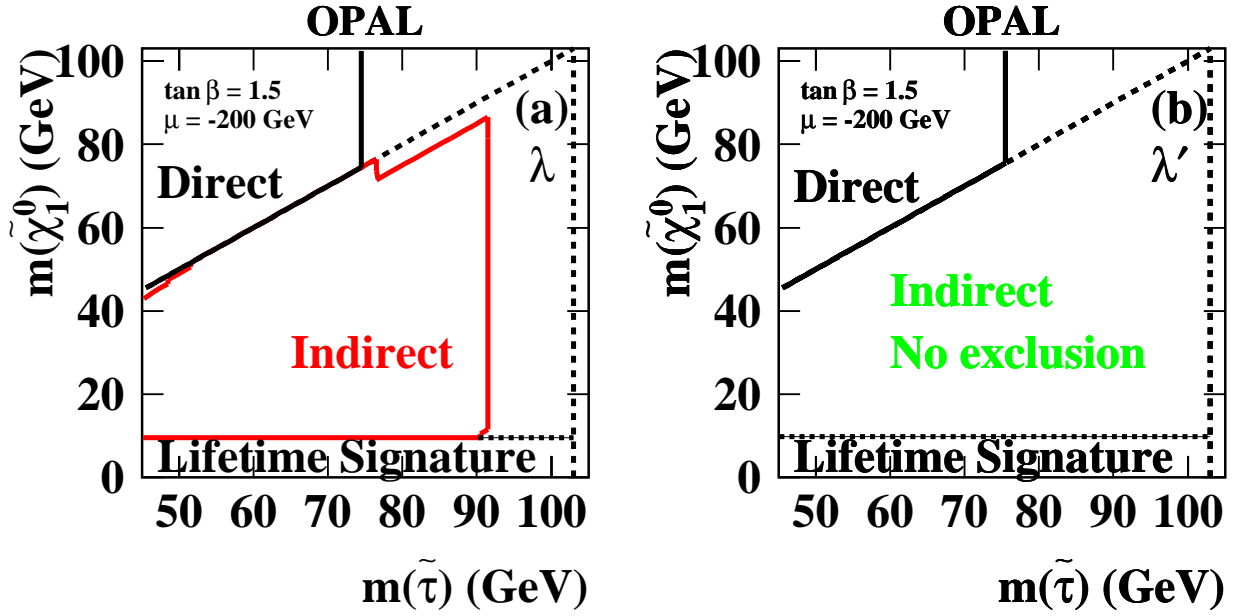
Figure 16: *CMSSM exclusion region for $\tilde{\tau}^+\tilde{\tau}^-$ production in the $(m_{\tilde{\tau}}, m_{\tilde{\chi}_1^0})$ plane at 95% C.L. for (a) a λ coupling and (b) a λ' coupling. For indirect decays via a λ' coupling, no exclusion was possible since the excluded experimental cross-section is always larger than the theoretical cross-sections. For direct decays, the exclusion region for $\tilde{\tau}_L\tilde{\tau}_L$ is shown. The kinematic limit is shown by the dashed lines.*
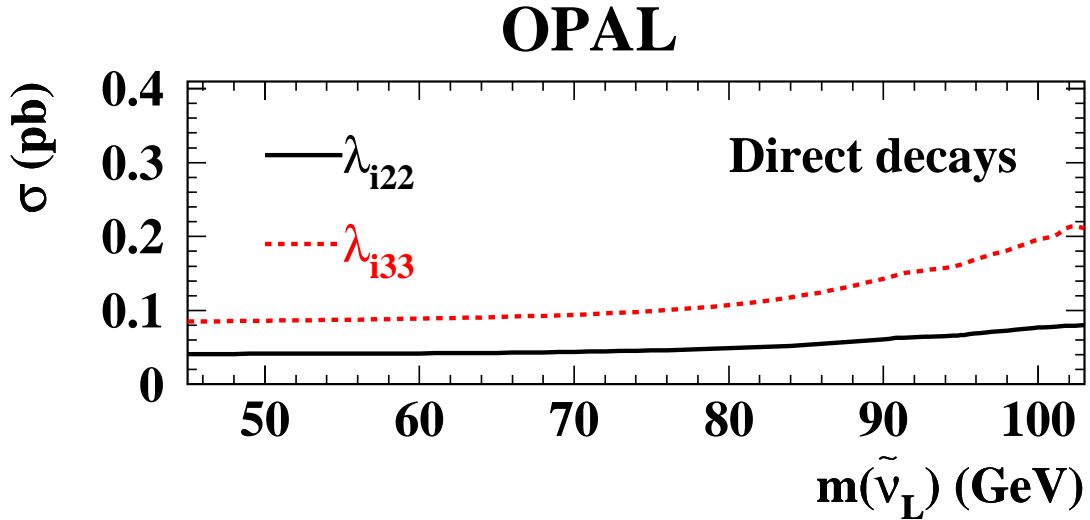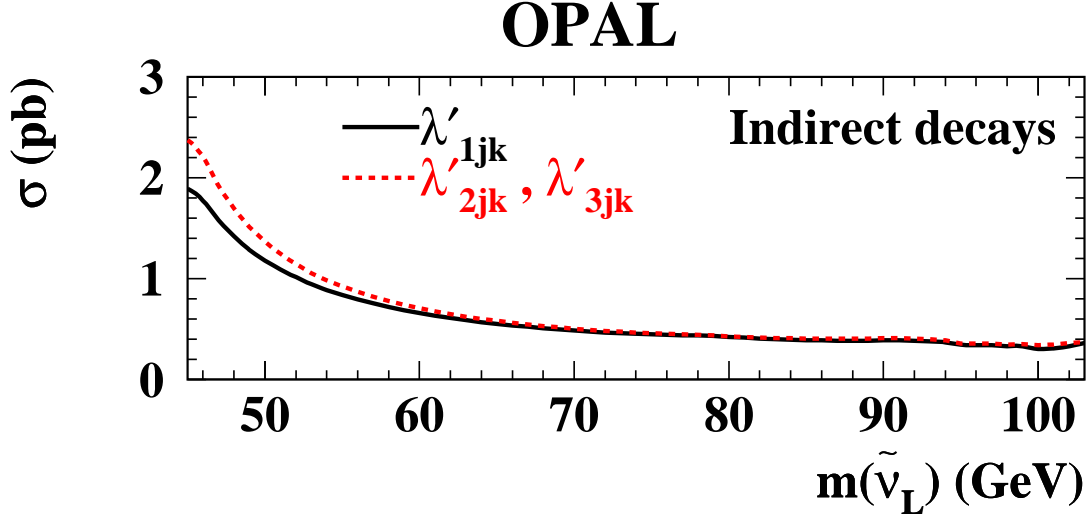

Figure 17: *Sneutrino direct decays via a λ coupling: upper limits at the 95% C.L. on the pair-production cross-sections of sneutrinos decaying directly. The dashed line shows the lowest upper limit (final states with four taus), while the solid line shows the highest one (final states with four muons).*

OPAL
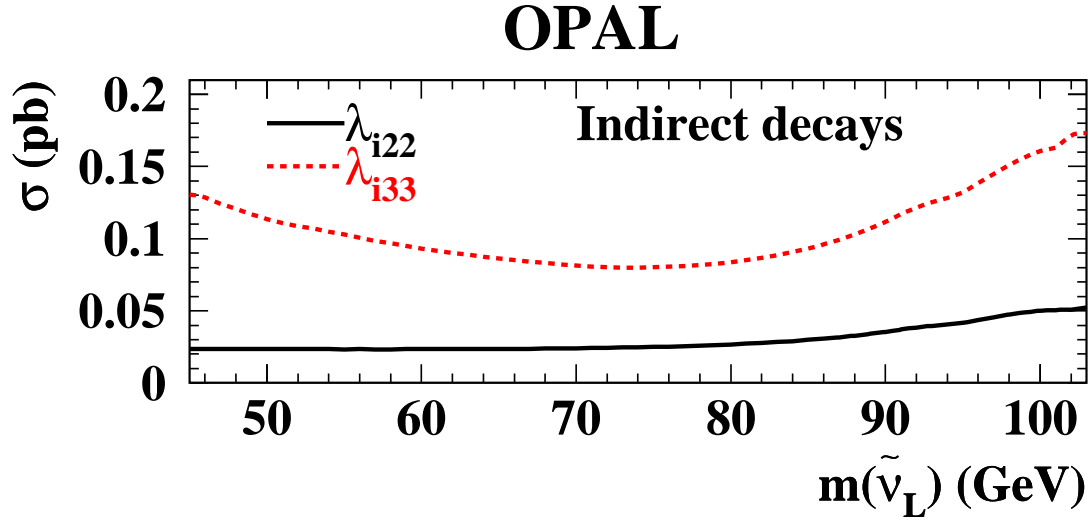
Figure 18: *Sneutrino indirect decays via a λ coupling: upper limits at the 95% C.L. on the pair-production cross-sections of sneutrinos decaying indirectly, for $\Delta m \leq m_{\tilde{\nu}}/2$. The dashed line shows the lowest upper limit (final states with 4 τ's and missing energy) while the solid line shows the highest one (final states with 4 μ's and missing energy).*
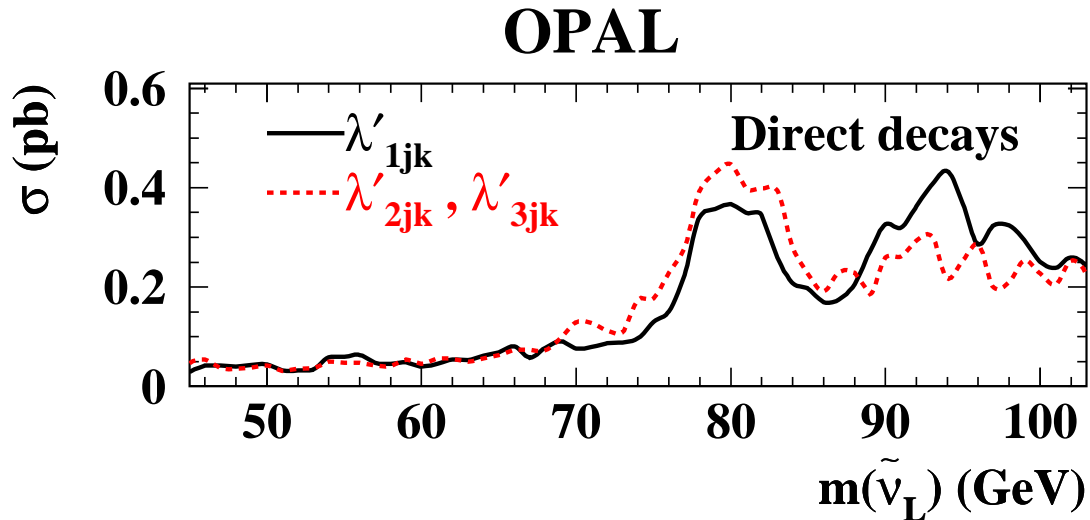
Figure 19: *Sneutrino direct decays via a λ' coupling: upper limits at the 95% C.L. on the pair-production cross-sections of $\tilde{\nu}_e$ (solid line) and $\tilde{\nu}_\mu/\tilde{\nu}_\tau$ (dashed line) decaying directly.*

These limits degrade for $\Delta m > m_{\tilde{\nu}}/2$ due to the larger fraction of missing energy and lower energy final state jets.

Figure 20: *Sneutrino indirect decays via a λ' coupling: upper limits at the 95% C.L. on the pair-production cross-sections of $\tilde{\nu}_e$ (solid line) and $\tilde{\nu}_\mu/\tilde{\nu}_\tau$ (dashed line), for $\Delta m \leq m_{\tilde{\nu}}/2$.*

In the CMSSM, the $\tilde{\nu}_e$ pair-production cross-section is enhanced by the presence of the t-channel diagram. The exclusion limits for $\tilde{\nu}_e$ decaying via a λ coupling are shown in Figure 21(a). For a low-mass $\tilde{\chi}_1^0$, this excluded region degrades due to a substantially smaller branching ratio for the decay $\tilde{\nu} \rightarrow \nu\tilde{\chi}_1^0$ but also due to a smaller detection efficiency for $\Delta m > m_{\tilde{\nu}}/2$. The exclusion limits for $\tilde{\nu}_e$ decaying via a λ' coupling are shown in Figure 21 (b). The lower mass limits for electron sneutrinos decaying directly or indirectly via a λ or a λ' coupling are summarised in Table 13.

Sneutrino Lower Mass Limits(GeV)				
Species	λ		λ'	
	Direct	Indirect	Direct	Indirect
$\tilde{\nu}_e$	89	95	89	88
$\tilde{\nu}_\mu/\tilde{\nu}_\tau$	79	81	74	-

Table 13: *Lower mass limits for sneutrinos decaying directly or indirectly via a λ or a λ' coupling. For the indirect decays, lower mass limits are quoted for a large-mass $\tilde{\chi}_1^0$ (60 GeV).*

Some combinations of neutralino and sneutrino masses do not correspond to points in the CMSSM parameter space for the specific choice of $\mu = -200$ GeV and $\tan\beta = 1.5$. Regions where this is the case are labelled "Theoretically not accessible" in the figures.

The theoretical cross-sections for $\tilde{\nu}_\mu$ and $\tilde{\nu}_\tau$ pair-production are smaller than for $\tilde{\nu}_e$. The exclusion limits for $\tilde{\nu}_\mu/\tilde{\nu}_\tau$ decaying via a λ coupling are shown in Figure 22(a).

The exclusion limits for $\tilde{\nu}_\mu/\tilde{\nu}_\tau$ decaying via a λ' coupling are shown in Figure 22 (b). No exclusion is possible for the indirect decays. The lower mass limits for muon/tau sneutrinos decaying directly via a λ or a λ' are summarised in Table 13.
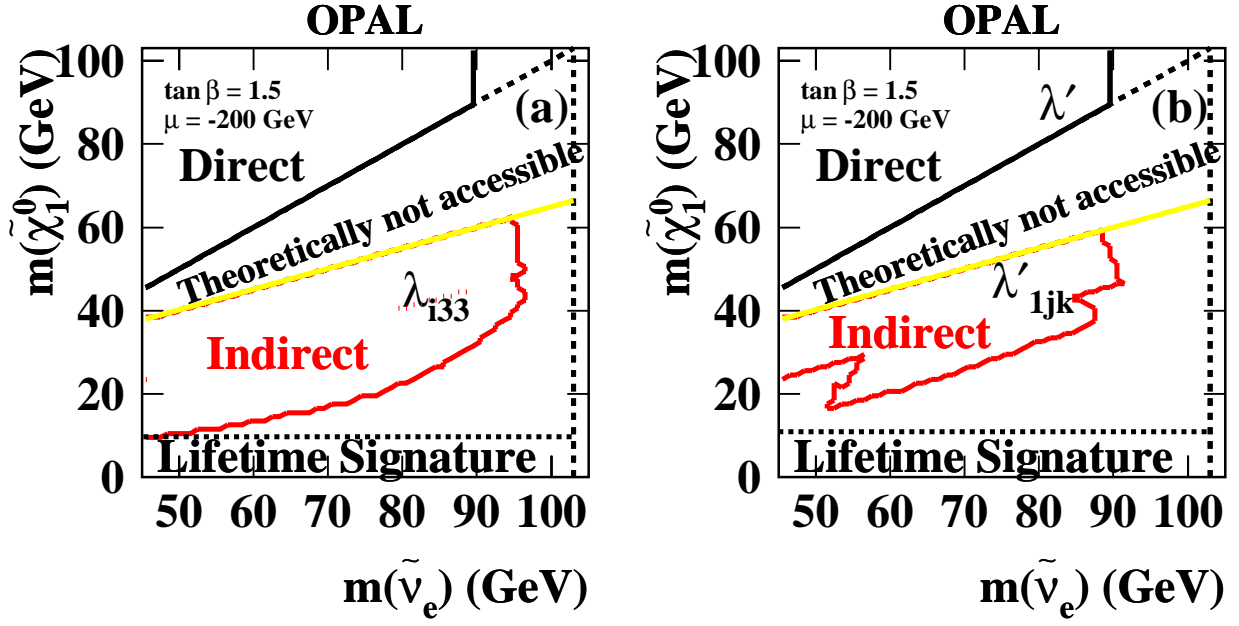
Figure 21: *CMSSM exclusion region for $\tilde{\nu}_e\tilde{\nu}_e$ production in the $(m_{\tilde{\nu}_e}, m_{\tilde{\chi}_1^0})$ plane at 95% C.L. for (a) a λ coupling and (b) a λ' coupling, assuming the CMSSM predicted branching ratio for the decay $\tilde{\nu}_e \to \nu_e\tilde{\chi}_1^0$. The kinematic limit is shown by the dashed lines.*
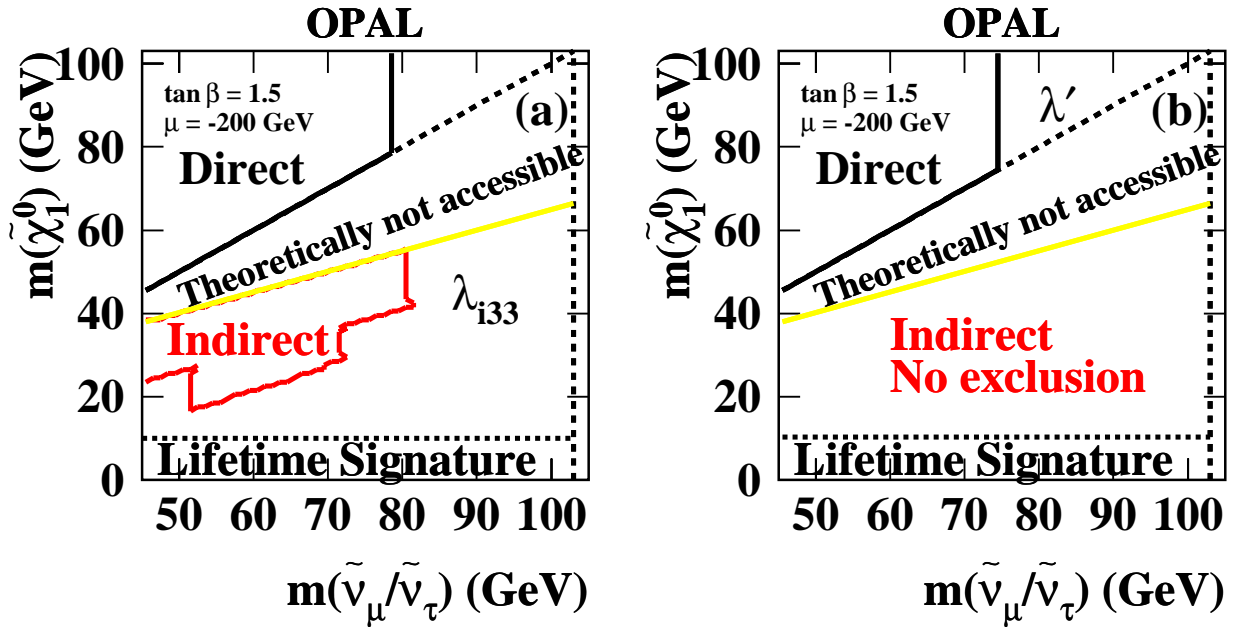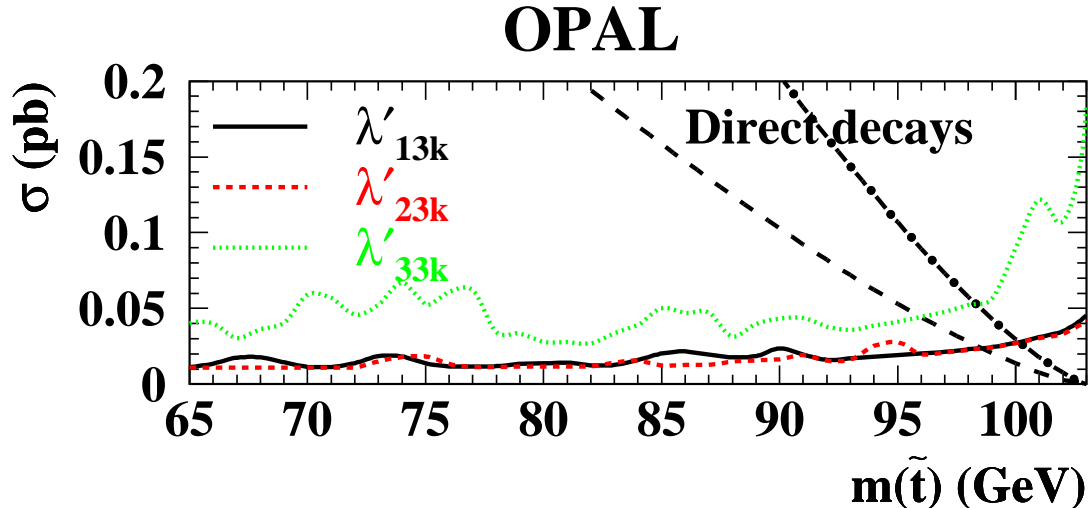

Figure 22: *CMSSM exclusion region for $\tilde{\nu}_\mu\tilde{\nu}_\mu$, $\tilde{\nu}_\tau\tilde{\nu}_\tau$ production in the $(m_{\tilde{\nu}}, m_{\tilde{\chi}_1^0})$ plane at 95% C.L. for (a) a λ coupling and (b) a λ' coupling, assuming the CMSSM predicted branching ratio for the decay $\tilde{\nu} \to \nu\tilde{\chi}_1^0$. The kinematic limit is shown as the dashed line.*

45

Figure 23: *Stop direct decays via a λ' coupling: upper limits at the 95% C.L. on the production cross-section of $\tilde{t}$ in the electron channel (solid line), the muon channel (short-dashed line) and in the tau channel (dotted line). Also shown are the maximum (dashed-dotted line) and minimum (long-dashed line) cross-sections predicted by the CMSSM, corresponding to mixing angles of 0 rad and 0.98 rad (decoupling limit).*

10.5   Stop limits

A cross-section limit of 0.03 pb was derived for the pair-production of stops decaying directly via λ'_{13k} or λ'_{23k} (electron and muon channels), in the mass region 45 GeV $< m_{\tilde{t}} <$ 100 GeV. The excluded cross-sections are shown in Figure 23 as a function of the stop mass for the electron, muon and tau channels.

If one assumes a stop production cross-section as predicted by the CMSSM, masses lower than 98 GeV can be excluded for any mixing angle $\theta_{\tilde{t}}$. A cross-section limit of 0.07 pb was derived for the pair-production of the stops decaying directly via λ'_{33k} (tau channel), in the mass region 45 GeV $< m_{\tilde{t}} <$ 100 GeV. In the tau channel, masses lower than 96 GeV can be excluded for any mixing angle $\theta_{\tilde{t}}$. More detailed exclusion limits are given in Table 14. The value of the mixing angle $\theta_{\tilde{t}} = 0.98$ rad corresponds to the decoupling of the stop from the Z^0 and gives the lowest stop pair-production cross-sections.

For the light squark decays via λ'' couplings, a cross-section limit of approximately 0.1 pb was derived for a squark mass up to $\approx$ 70 GeV. This limit degrades to 0.39 pb in the range of the W mass as shown in Figure 24. Assuming the same detection efficiencies for the stop quarks as for the simulated light squarks, a limit on the stop mass can be established. If the stop production cross-section predicted by the CMSSM is assumed, masses lower than 77 GeV can be excluded for any mixing angle $\theta_{\tilde{t}}$.

11   Conclusions

A search was performed for pair-produced sfermions with R-parity violating decays using the data collected by the OPAL detector at centre-of-mass energies of $189-209$ GeV, corresponding

Stop Lower Mass Limits (GeV)		
Channels	$\theta_{\tilde{t}}$	
	0 rad	0.98 rad
$\tilde{t}_1 \rightarrow e+q$	100	98
$\tilde{t}_1 \rightarrow \mu+q$	100	98
$\tilde{t}_1 \rightarrow \tau+q$	98	96
$\tilde{t}_1 \rightarrow qq$	88	77

Table 14: *Stop lower mass limits for the two extreme values of the mixing angle in the electron, muon and tau channels as well as in the 4-jet channel.*
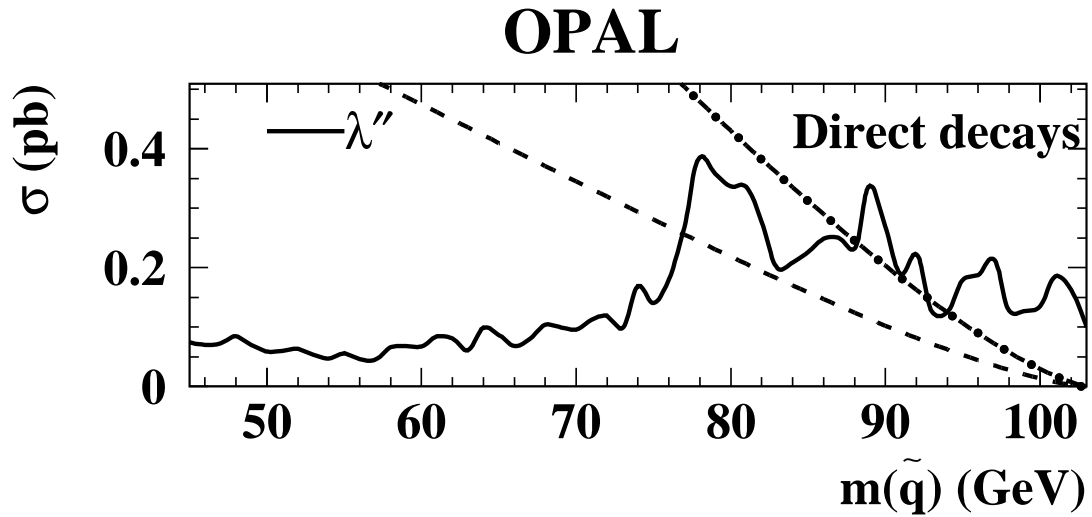

Figure 24: *Squark direct decays via a λ'' coupling: upper limits at the 95% C.L. on the production cross-section of squarks decaying directly. Also shown are the maximum (dashed-dotted line) and minimum (dashed line) stop production cross-sections predicted by the CMSSM, corresponding to mixing angles of 0 rad and 0.98 rad.*

to a total luminosity of approximately 610 pb^{-1}. Direct and indirect R-parity violating decay modes of $\tilde{\ell}$ and $\tilde{\nu}$ via the Yukawa λ and λ' couplings were considered, as well as direct R-parity violating decay modes of $\tilde{t}$ and $\tilde{q}$ via λ' and λ''.

No significant excess of signal-like events was observed in the data. Upper limits on the pair-production cross-sections for sfermions have been computed assuming that only R-parity violating decays occur. These cross-section limits depend only on the masses of the sfermions and not on other SUSY parameters. Mass limits were derived in the framework of the Constrained Minimal Supersymmetric Standard Model whenever the predicted cross-sections were sufficiently large.

Acknowledgements

References

[1] Y. Gol'fand and E. Likhtam, JETP Lett. **13** (1971) 323;
D. Volkov and V. Akulov, Phys. Lett. **B46** (1973) 109;
J. Wess and B. Zumino, Nucl. Phys. **B70** (1974) 39.

[2] H.P. Nilles, Phys. Rep. **110** (1984) 1;
H.E. Haber and G.L. Kane, Phys. Rep. **117** (1985) 75.

[3] P. Fayet, in *"Unification of the Fundamental Particle Interactions"*, eds. S. Ferrara, J. Ellis and P. Van Nieuwenhuizen, Plenum Press (1980) 727.

[4] S. Dimopoulos and L.J. Hall, Phys. Lett. **B207** (1988) 210;
J. Erler, J.L. Feng and N. Polonsky, Phys. Rev. Lett. **78** (1997) 3063;
J.Kalinowski, R. Ruckl, H.Spiesberger and P.M. Zerwas, Phys. Lett. **B406** (1997) 314.

[5] V. Barger, G.F. Giudice and T. Han, Phys. Rev. **D40** (1989) 2987.

[6] H. Dreiner, *"An Introduction to Explicit R-parity Violation"*, in *"Perspectives on Super-symmetry"*, ed. G.L. Kane (1997) 462, hep-ph/9707435.

[7] R.N. Mohapatra, Phys. Rev. **D34** (1986) 3457.

[8] R.M. Godbole, P. Roy and T. Tata, Nucl. Phys. **B401** (1993) 67.

[9] G. Bhattacharyya, J. Ellis and K. Sridhar, Mod. Phys. Lett. **A10** (1995) 1583.

[10] J.L. Goity and M. Sher, Phys. Lett. **B346** (1995) 69.

[11] M. Hirsh, H. V. Klapdor-Kleingrothaus and S. G. Kovalenko, Phys. Rev. Lett. **75** (1995) 17.

[12] K. Agashe and M. Graesser, Phys. Rev. **D54** (1996) 4445.

[13] A.Y. Smirnow and F. Vissani, Phys. Lett. **B380** (1996) 317.

[14] G. Bhattacharyya, *"R-parity Violating Supersymmetric Yukawa Couplings: a Mini-Review,"* Nucl. Phys. Proc. Suppl. **A52** (1997) 83.

[15] B.C. Allanach, A. Dedes and H. Dreiner, Phys. Rev. **D60** (1999) 075014.

[16] OPAL Collab., G. Abbiendi *et al.*, Eur. Phys. J. **C12** (2000) 1.

[17] OPAL Collab., K. Ackerstaff *et al.*, Phys. Lett. **B433** (1998) 195;
OPAL Collab., G. Abbiendi *et al.*, Eur. Phys. J. **C14** (2000) 187; OPAL Collab., G. Abbiendi *et al.*, accepted by Phys. Lett. .

[18] ALEPH Collab., R. Barate *et al.*, *"Search for Supersymmetric Particles with R-Parity Violating Decays in e^+e^- Collisions at $\sqrt{s}$ up to 209 GeV"*, CERN-EP-2002-071, submitted to the Eur. Phys. J. C;
DELPHI Collab., P. Abreu *et al.*, Phys. Lett. **B487** (2000) 36;
DELPHI Collab., P. Abreu *et al.*, Phys. Lett. **B500** (2001) 22;
L3 Collab., M. Acciarri *et al.*, Eur. Phys. J. **C19** (2001) 397.

[19] CDF Collab., F. Abe *et al.*, Phys. Rev. Lett. **83** (1999) 2133.

[20] D0 Collab., B. Abbott *et al.*, Phys. Rev. Lett. **83** (1999) 4476;
D0 Collab., B. Abbott *et al.*, Phys. Rev. **D62** (2000) 071701.

[21] H1 Collab., C. Adloff *et al.*, Eur. Phys. J. **C20** (2001) 639.

[22] ZEUS Collab., J. Breitweg *et al.*, Eur. Phys. J. **C16** (2000) 253;
ZEUS Collab., J. Breitweg *et al.*, Phys. Rev. **D63** (2001) 052002.

[23] OPAL Collab., K. Ackerstaff *et al.*, Eur. Phys. J. **C2** (1998) 441;
OPAL Collab., G. Abbiendi *et al.*, Eur. Phys. J. **C6** (1999) 1.

[24] OPAL Collab., K. Ahmet *et al.*, Nucl. Instr. Meth. **A305** (1991) 275;
P.P. Allport *et al.*, Nucl. Instr. Meth. **A324** (1993) 34;
P.P. Allport *et al.*, Nucl. Instr. Meth. **A346** (1994) 476.

[25] S. Anderson *et al.*, Nucl. Instr. and Meth. **A403** (1998) 326.

[26] G. Aguillion *et al.*, Nucl. Instr. and Meth. **A417** (1998) 266.

[27] B.E. Anderson *et al.*, IEEE Transactions on Nuclear Science **41** (1994) 845.

[28] OPAL Collab., G. Abbiendi *et al.*, Eur. Phys. J. **C26** (2003) 479.

[29] OPAL Collab., M.Z. Akrawy *et al.*, Phys. Lett. **B253** (1991) 511.

[30] J. Allison *et al.*, Nucl. Instr. Meth. **A317** (1992) 47.

[31] S. Katsanevas and S. Melachroinos, in *"Physics at LEP2"*, eds. G. Altarelli, T. Sjöstrand and F. Zwirner, CERN 96–01, vol. 2, p. 328;
S. Katsanevas and P. Morawitz, Comp. Phys. Comm. **112** (1998) 227.

[32] T. Sjöstrand and M. Bengtsson, Comp. Phys. Comm. **43** (1987) 367;
"PYTHIA 5.7 and JETSET 7.4, Physics and Manual", CERN–TH. 7112/93;
T. Sjöstrand, Comp. Phys. Comm. **82** (1994) 74.

[33] B. Andersson, G. Gustafson, G. Ingelman and T. Sjöstrand, Phys. Rep. **97** (1983) 31.

[34] OPAL Collab., K. Ackerstaff *et al.*, Z. Phys. **C75** (1997) 409.

[35] C. Peterson, D. Schlatter, I. Schmitt and P.M. Zerwas, Phys. Rev. **D27** (1983) 105.

[36] R. Engel and J. Ranft, Phys. Rev. **D54** (1996) 4244;
R. Engel, Z. Phys. **C66** (1995) 203.

[37] G. Marchesini *et al.*, Comp. Phys. Comm. **67** (1992) 465.

[38] R. Bhattacharya, J. Smith and G. Grammer, Phys. Rev. **D15** (1977) 3267;
J. Smith, J.A.M. Vermaseren and G. Grammer, Phys. Rev. **D15** (1977) 3280.

[39] J. Fujimoto *et al.*, Comp. Phys. Comm. **100** (1997) 128.

[40] S. Jadach, Comp. Phys. Comm. **140** (2001) 475.

[41] S. Jadach, W. Placzek, M. Skmzyoek, B.F.L. Ward and Z. Was, Comp. Phys. Comm. **140** (2001) 432.

[42] S. Jadach, Phys. Rev. **D61** (2000) 113010;
S. Jadach, Comp. Phys. Comm. **140** (2001) 432.

[43] S. Jadach *et al.*, in *"Physics at LEP2"*, eds. G. Altarelli, T. Sjöstrand and F. Zwirner, CERN 96–01, vol.2, p. 229;
S. Jadach, W. Placzek and B.F.L. Ward, Phys. Lett. **B390** (1997) 298.

[44] S. Jadach, B.F.L. Ward and Z. Wąs, Comp. Phys. Comm. **79** (1994) 503.

[45] S. Jadach, B.F.L. Ward and Z. Wąs, Comp. Phys. Comm. **130** (2000) 260.

[46] OPAL Collab., K. Ackerstaff *et al.*, Phys. Lett. **B396** (1997) 301.

[47] OPAL Collab., G. Alexander *et al.*, Z. Phys. **C70** (1996) 357.

[48] OPAL Collab., R. Akers *et al.*, Phys. Lett. **B327** (1994) 411.

[49] OPAL Collab., R. Akers *et al.*, Z. Phys. **C60** (1993) 199.

[50] OPAL Collab., P.D. Acton *et al.*, Z. Phys. **C60** (1993) 19.

[51] OPAL Collab., R. Akers *et al.*, Z. Phys. **C61** (1994) 19.

[52] OPAL Collab., K. Ackerstaff *et al.*, Phys. Lett. **B389** (1996) 416.

[53] OPAL Collab., K. Ackerstaff *et al.*, Eur. Phys. J. **C7** (1999) 407.

[54] N. Brown and W.J. Stirling, Phys. Lett. **B252** (1990) 657;
S. Catani *et al.*, Phys. Lett. **B269** (1991) 432;
S. Bethke, Z. Kunszt, D. Soper and W.J. Stirling, Nucl. Phys. **B370** (1992) 310;
N. Brown and W.J. Stirling, Z. Phys. **C53** (1992) 629.

[55] OPAL Collab., K. Ackerstaff *et al.*, Eur. Phys. J. **C6** (1999) 225.

[56] M.G. Bowler, Z. Phys. **C11** (1981) 169.

[57] OPAL Collab., K. Ackerstaff *et al.*, Eur. Phys. J. **C2** (1998) 441.

[58] OPAL Collab., K. Ackerstaff *et al.*, Euro. Phys. J. **C5** (1998) 19.

[59] OPAL Collab., G. Alexander *et al.*, Phys. Lett. **B376** (1996) 232.

[60] R.K. Ellis, D.A. Ross and A.E. Terrano, Nucl. Phys. **B178** (1981) 421.

[61] A.G. Frodesen, O. Skeggestad, and H. Tofte, *"Probability and Statistics in Particle Physics"*, Universitetsforlaget, 1979, ISBN 82-00-01-01906-3;
S.L. Meyer, *"Data Analysis for Scientists and Engineers"*, John Wiley and Sons, 1975.